



**UNIVERSITY OF LEEDS**

This is a repository copy of *The Effect of Atmospheric Acid Processing on the Global Deposition of Bioavailable Phosphorus from Dust*.

White Rose Research Online URL for this paper:  
<http://eprints.whiterose.ac.uk/134565/>

Version: Accepted Version

---

**Article:**

Herbert, RJ, Krom, MD, Carslaw, KS [orcid.org/0000-0002-6800-154X](https://orcid.org/0000-0002-6800-154X) et al. (5 more authors) (2018) The Effect of Atmospheric Acid Processing on the Global Deposition of Bioavailable Phosphorus from Dust. *Global Biogeochemical Cycles*, 32 (9). pp. 1367-1385. ISSN 0886-6236

<https://doi.org/10.1029/2018GB005880>

---

©2018. American Geophysical Union. All Rights Reserved. This is an author produced version of a paper published in *Global Biogeochemical Cycles*. Uploaded in accordance with the publisher's self-archiving policy.

**Reuse**

Items deposited in White Rose Research Online are protected by copyright, with all rights reserved unless indicated otherwise. They may be downloaded and/or printed for private study, or other acts as permitted by national copyright laws. The publisher or other rights holders may allow further reproduction and re-use of the full text version. This is indicated by the licence information on the White Rose Research Online record for the item.

**Takedown**

If you consider content in White Rose Research Online to be in breach of UK law, please notify us by emailing [eprints@whiterose.ac.uk](mailto:eprints@whiterose.ac.uk) including the URL of the record and the reason for the withdrawal request.



[eprints@whiterose.ac.uk](mailto:eprints@whiterose.ac.uk)  
<https://eprints.whiterose.ac.uk/>

1 | **The Effect of Atmospheric Acid Processing on the Global Deposition of Bioavailable**  
2 **Phosphorus from Dust**

3 **R. J. Herbert<sup>1,†</sup>, M. D. Krom<sup>1,‡</sup>, K. S. Carslaw<sup>1</sup>, A. Stockdale<sup>1</sup>, R. J. G. Mortimer<sup>2</sup>, L. G.**  
4 **Benning<sup>1,3,4</sup>, K. Pringle<sup>1</sup>, J. Browse<sup>1,\*</sup>**

5 <sup>1</sup> School of Earth and Environment, University of Leeds, Leeds, LS2 9JT, UK.

6 <sup>2</sup> School of Animal, Rural and Environmental Sciences, Nottingham Trent University,  
7 Brackenhurst Campus, Southwell, Nottinghamshire, NG25 0QF, UK.

8 <sup>3</sup> GFZ German Research Centre for Geosciences, Telegrafenberg, 14473 Potsdam, Germany.

9 <sup>4</sup> Department of Earth Sciences, Free University of Berlin, 12249 Berlin, Germany.

10

11 Corresponding author: Ross Herbert ([r.j.herbert@reading.ac.uk](mailto:r.j.herbert@reading.ac.uk))

12

13 † Now at Department of Meteorology, University of Reading, Reading, RG6 6AH, UK.

14 ‡ Now at Morris Kahn Marine Research Station, Department of Marine Biology, Leon H.  
15 Charney School of Marine Science, University of Haifa, Haifa, 3498838, Israel.

16 \* Now at College of Life and Environmental Sciences, University of Exeter, Penryn, TR10 9EZ,  
17 UK.

18

Formatted: Numbering: Continuous

19 **Abstract**

20 The role of dust as a source of bioavailable phosphorus (Bio-P) is quantified using a new  
21 parameterization for apatite dissolution in combination with global soil data maps and a global  
22 aerosol transport model. Mineral dust provides 31.2 Gg-P yr<sup>-1</sup> of Bio-P to the oceans, with  
23 14.3 Gg-P yr<sup>-1</sup> from labile P present in the dust, and an additional 16.9 Gg-P yr<sup>-1</sup> from acid  
24 dissolution of apatite in the atmosphere, representing an increase of 120%. The North Atlantic,  
25 northwest Pacific, and Mediterranean Sea are identified as important sites of Bio-P deposition  
26 from mineral dust. The acid dissolution process increases the fraction of total-P that is  
27 bioavailable from ~10% globally from the labile pool to 23% in the Atlantic Ocean, 45% in the  
28 Pacific Ocean, and 21% in the Indian Ocean, with an ocean global mean value of 22%. Strong  
29 seasonal variations, especially in the North Pacific, northwest Atlantic, and Indian Ocean, are  
30 driven by large-scale meteorology and pollution sources from industrial and biomass-burning  
31 regions. Globally constant values of total-P content and bioavailable fraction used previously do  
32 not capture the simulated variability. We find particular sensitivity to the representation of  
33 particle-to-particle variability of apatite, which supplies Bio-P through acid-dissolution, and  
34 calcium carbonate, which helps to buffer the dissolution process. A modest 10% external mixing  
35 results in an increase of Bio-P deposition by 18%. The total Bio-P calculated here  
36 (31.2 Gg-P yr<sup>-1</sup>) represents a minimum compared to previous estimates due to the relatively low  
37 total-P in the global soil map used.

38  
39

## 40 **1 Introduction**

41 Phosphorus (P) is an essential requirement for life. In the terrestrial ecosystem P is made  
42 accessible naturally through weathering processes and increasingly through the supply of  
43 fertilizer and other P-containing compounds from anthropogenic processes. The dominant supply  
44 of P to coastal systems is from rivers and wastewater discharge, which are augmented by  
45 sedimentary recycling processes (Ruttenberg, 2003). By contrast, in the offshore ocean the  
46 dominant external supply is from atmospheric deposition processes, with long-range  
47 transportation of mineral dust from desert regions being the most important single source of P to  
48 the ocean surface (Graham and Duce, 1982; Mahowald et al., 2008; Myriokefalitakis et al.,  
49 2016). In-situ measurements of atmospheric aerosol (e.g., Carbo et al., 2005; Herut et al., 1999;  
50 Zamora et al., 2013) and soil mineralogical databases (Nickovic et al., 2012; Yang et al., 2013)  
51 show that total P (hereafter TP) content of soils and mineral dust is spatially and temporally  
52 variable and may range from < 500 to > 1000 ppm, with corresponding variability in the  
53 component P pools.

54  
55 Many studies show the importance of atmospheric supply in general and dust in particular as a  
56 source of external nutrients (Fe, N and P) to the open ocean (Krishnamurthy et al., 2010;  
57 Mahowald et al., 2008). In such systems, the total N supplied is in a readily bioavailable form. In  
58 contrast the P (and Fe) is supplied in both labile (and hence bioavailable) and non-bioavailable  
59 forms. The non-bioavailable particles of P can drop through the photic zone without enhancing  
60 phytoplankton growth and hence carbon uptake. Herut et al. (2005) showed that when fresh  
61 Saharan dust and dust pre-treated to remove any water-leachable nutrients were added to a  
62 microcosm experiment containing N- and P-limited Mediterranean seawater only the fresh dust  
63 resulted in increased chlorophyll content. The fresh dust added nutrients in the ratio of 31N:1P  
64 (nitrate:phosphate) and thus it was the water-leachable fraction of the dust rather than the particle  
65 itself that caused the extra productivity in this N and P co-limited system (Thingstad et al.,  
66 2005). Eijssink et al. (2000) found that even in the P-limited Eastern Mediterranean, 70% of the  
67 TP (mainly detrital apatite) supplied as Saharan dust to the surface waters was transferred  
68 through the water column and ended up deposited in the sediment. The remaining 30% was taken  
69 up by biological processes in the water column.

70  
71 Observations suggest that the percentage of TP in mineral dust that is deposited in a bioavailable  
72 form (Bio-P) is spatially variable, ranging from < 10% to > 80% (Baker et al., 2006a; Markaki et  
73 al., 2003; Zamora et al., 2013; Vet et al., 2014), and may increase with distance from the dust  
74 source (Baker et al., 2006a). Recent ambient observations and laboratory experiments (Nenes et  
75 al., 2011; Srinivas and Sarin, 2015; Stockdale et al., 2016) provide support for the hypothesis  
76 that atmospheric acidification and subsequent dissolution is a primary process for producing Bio-  
77 P in mineral dust. Increasing the amount of leachable, or bioavailable, P by acid processes in the  
78 atmosphere will have a direct effect of increasing phytoplankton biomass and hence carbon  
79 uptake in a variety of ocean systems (e.g., Jickells and Moore, 2015; Mahowald et al., 2008)

80  
81 The paucity of observational data from the open oceans necessitates the use of models to  
82 determine the atmospheric flux of Bio-P to surface waters. Models are also needed to quantify  
83 how Bio-P deposition may change with environmental factors such as source strength,  
84 atmospheric pollution, and large-scale changes to global circulation. To achieve this, models  
85 must represent the emission, transport and deposition of the particulate P, as well as processes

86 that determine the TP and Bio-P content. Previous global deposition modelling studies using  
87 global chemical transport models (Brahney et al., 2015; Krishnamurthy et al., 2010; Mahowald  
88 et al., 2008; Wang et al., 2015) assumed that dust emissions contain a constant fraction of TP  
89 (between ~720 and 1050 ppm) and a constant percentage of TP deemed Bio-P (between 10% and  
90 15%). The result is a spatially varying flux of dust-borne P to the surface with a constant  
91 solubility, which may not reflect underlying variability between dust sources, nor atmospheric  
92 acidification processes. A recent study by Myriokefalitakis et al. (2016) represented the  
93 acidification process using an acid-solubilization mechanism in which apatite dissolution is  
94 treated as a kinetic process dependent on the  $H^+$  activity of the surrounding water droplet and  
95 known acid dissolution thermodynamic constants. Their study used a global soil mineralogy  
96 dataset (Nickovic et al., 2012) to represent the spatially varying soil TP content with dust-TP  
97 emissions adjusted to a global mean of 880 ppm and a soluble fraction of 10% representing a  
98 leachable inorganic pool of P in the initial dust. The remaining TP was assumed to be apatite.  
99 This treatment reproduces the atmospheric acidification process but relies on several  
100 assumptions for estimating the different forms of P. A recent global soil database (Yang et al.,  
101 2013) provides high resolution information on the geographical distribution of TP in its different  
102 forms including apatite, labile, organic, occluded, and secondary P. The dataset shows that there  
103 is considerable spatial variability in all components. This dataset provides more appropriate  
104 forms of P for use in estimating dust-borne P emissions and simulating atmospheric acidification  
105 processes of apatite.

106  
107 A recent study by Stockdale et al. (2016) presents results from a series of experiments simulating  
108 atmospheric acidification on dust samples and dust precursor soils in which the acidity of the  
109 solution and the mass of dust was systematically varied. Phosphorus speciation experiments  
110 identified the dominant forms of phosphorus in the dust samples as ~80% apatite P, ~10% Fe-  
111 bound P, and ~10% labile-P. The acidification experiments provide robust evidence for a  
112 relatively simple relationship in which the dissolution behaviour of mineral dust is controlled by  
113 the absolute number of protons in the solution, the calcium carbonate ( $CaCO_3$ ) content, and the  
114 apatite (Ap-P) content of the dust. Rapid acid dissolution of both mineral species occurs  
115 simultaneously when both minerals are present on the same mineral grain (internally mixed). The  
116 dissolution rate of Ap-P is greater when the Ap-P and  $CaCO_3$  exist on different grains (externally  
117 mixed). As a result of slow mineral precipitation kinetics the dissolved phosphate remains in  
118 solution when the  $H^+$  concentration falls or water content increases. The total mass of Bio-P  
119 upon deposition to the surface is thus the sum of acid-dissolved apatite (Acid-P) and the loosely  
120 bound labile P (Lab-P) that was initially available in the particles. As the dissolution of Ap-P  
121 occurs at a faster rate when  $CaCO_3$  is not present, if Ap-P and  $CaCO_3$  were exclusively present  
122 on different particles (i.e., externally mixed) then it is possible that more Acid-P would be  
123 produced. As discussed by Stockdale et al. (2016) it is hypothesized that many particles would  
124 contain both Ap-P and  $CaCO_3$ , however, there is likely a degree of variation between particles  
125 with some containing more or less of each mineral component.

126  
127 It is widely recognized that mineral dust plays an important role in the transport of nutrients to  
128 the open ocean surfaces, however, as shown by Yang et al. (2013) there exists considerable  
129 variability in the relative abundance of different P-containing components from different source  
130 regions. The results of Stockdale et al. (2016) additionally show that the spatial distribution of  
131  $CaCO_3$  and its abundance in relation to Ap-P may have considerable impacts on the production

132 of Bio-P from acid dissolution of Ap-P. The simplistic dissolution mechanism presented by  
133 Stockdale et al. (2016) and the detailed soil-P speciation dataset presented by Yang et al. (2013)  
134 provide a new and readily applicable method for estimating the spatio-temporal distribution of  
135 Bio-P from dust and allows us to investigate the sensitivity of Acid-P production to the degree of  
136 internal and external mixing of the components. This will help to understand key uncertainties in  
137 the acid dissolution process and help better define the focus of future research.

138  
139 In this study we use the Global Model of Aerosol Processes (GLOMAP) coupled to the global  
140 chemical transport model TOMCAT to simulate the emission, transport, and deposition of dust-  
141 borne phosphorus to the surface. Apatite dissolution parameterizations based on the results from  
142 Stockdale et al. (2016) and a database of soil P speciation (Yang et al., 2013) are used to  
143 simulate atmospheric acidification of mineral dust by H<sub>2</sub>SO<sub>4</sub> and HNO<sub>3</sub>; the soil database is also  
144 used to simulate the contribution of the dust-borne Lab-P as a spatially variable percentage of  
145 dust mass. These results are used to investigate the drivers of the spatio-temporal variability in  
146 dust-borne Bio-P and the Acid-P (the amount of TP converted to Bio-P by atmospheric acid  
147 processes). The results are compared to a global dataset of observations (Vet et al., 2014) and  
148 results from other modelling studies to help understand the importance of atmospheric  
149 acidification of mineral dust on the global supply of P nutrients to the open oceans and  
150 elsewhere. Finally, simulations are performed to investigate the sensitivity of the results to the  
151 effect of external mixing of apatite and CaCO<sub>3</sub> on the amount of Bio-P delivered to the ocean  
152 surface.

153

## 154 **2 Model description**

155 We use the global aerosol microphysics model GLOMAP-mode (Mann et al., 2010) coupled to  
156 the 3D global chemical transport model TOMCAT (Chipperfield, 2006). Simulations are  
157 performed using a horizontal resolution of 2.8° by 2.8° and 31 hybrid  $\sigma$ -pressure levels extending  
158 from the surface to 10 hPa. Meteorology for the simulated year is driven by the European Centre  
159 for Medium-Range Weather Forecasts (ECMWF) ERA-Interim reanalyses at 6-hourly intervals  
160 Monthly mean low-cloud fields are prescribed from the International Satellite Cloud  
161 Climatology Project (ISCCP) archive. In the standard GLOMAP-mode setup the aerosol particle  
162 number and size distribution is described using a modal scheme with 7 internally mixed modes  
163 (4 soluble and 3 insoluble) and 5 aerosol species: sulfate, black carbon, organic carbon, sea-salt,  
164 and dust. The 7 modes cover four size ranges: nucleation (~1 to 10 nm diameter), Aitken (~10 to  
165 100 nm), accumulation (~0.1 to 0.5  $\mu$ m), and coarse (~0.5 to 10  $\mu$ m).

166  
167 The aerosol processes treated in the model include primary and precursor emissions, nucleation  
168 of H<sub>2</sub>SO<sub>4</sub> aerosol, sedimentation and dry deposition, hygroscopic growth, in-cloud activation and  
169 scavenging, below-cloud scavenging, inter- and intra-modal coagulation, condensation of H<sub>2</sub>SO<sub>4</sub>  
170 and secondary organic vapors onto all aerosol particles, ageing of water-insoluble particles, and  
171 in-cloud processing (formation of sulfate mass from oxidation of sulfur dioxide in aerosol  
172 particles activated into cloud droplets). GLOMAP-mode also includes an aerosol precursor  
173 chemistry scheme primarily for simulating gas and aqueous phase reactions leading to the  
174 production of SO<sub>2</sub> and H<sub>2</sub>SO<sub>4</sub>.

175

176 Monthly emissions of anthropogenic BC, OC, and SO<sub>2</sub>, and volcanic SO<sub>2</sub> are supplied by global  
177 datasets from AeroCom hindcast (Diehl et al., 2012). The Global Fire Emissions Database  
178 (GFED) v2 database (van der Werf et al., 2010) is used for wildfire emissions, and dimethyl  
179 sulfide (DMS) emissions are calculated using DMS seawater concentrations from Kettle et al.  
180 (1999) and transfer velocity parameterizations of Nightingale et al. (2000). Daily size-resolved  
181 emissions of dust (covering accumulation and coarse modes) are included via prescribed fluxes  
182 from AeroCom (Dentener et al., 2006). Deposition of aerosol species occurs via dry deposition,  
183 using a dry deposition velocity following Slinn (1982), and wet deposition through nucleation  
184 scavenging from large-scale and convective precipitation (activation of cloud condensation  
185 nuclei), impaction scavenging by precipitation, and scavenging by low-cloud drizzle (Browse et  
186 al., 2012). The aqueous chemistry scheme includes the dissolution of SO<sub>2</sub>, H<sub>2</sub>O<sub>2</sub>, and O<sub>3</sub> into  
187 cloud droplets and the subsequent oxidation of S(IV) to S(VI) by H<sub>2</sub>O<sub>2</sub> and O<sub>3</sub>. Condensation of  
188 H<sub>2</sub>SO<sub>4</sub> onto aerosols is simulated using coefficients following Fuchs and Sutugin (1971) with  
189 added correction factors for molecular effects and limiting interfacial mass transport, the latter  
190 using an accommodation coefficient 1.0 for both insoluble and soluble modes as per Mann et al.  
191 (2010). For this study, the condensation of HNO<sub>3</sub> onto dust has been added following the above  
192 method; HNO<sub>3</sub> concentrations are taken from the coupled TOMCAT model with condensation  
193 acting as a sink to the HNO<sub>3</sub> fields. For simplicity, the condensed HNO<sub>3</sub> is added to the sulfate  
194 component as an equivalent mass of H<sub>2</sub>SO<sub>4</sub> that would produce the same mass of H<sup>+</sup> ions upon  
195 dissociation of HNO<sub>3</sub>.

196  
197 In this study we are interested in the sulfate associated with dust aerosol, rather than the sulfate  
198 associated with sea-salt, and thus have altered the model setup to isolate the dust-associated  
199 sulfate which will be used to determine the amount of associated acid. Full details can be found  
200 in the supporting information (Text S1). The resulting annual dust deposition flux, shown  
201 alongside the data from the standard setup, is compared to AeroCom observations (Huneeus et  
202 al., 2011) in the supporting information (Figure S1) and shows the current setup is able to  
203 simulate dust deposition fluxes both close to source and in remote regions and is comparable to  
204 the original GLOMAP setup.

205  
206 To simulate the acid dissolution process in GLOMAP two soil databases were used to provide  
207 information on the dust mineralogy. For the different forms of P in the dust the soil phosphorus  
208 database presented by Yang et al. (2013) was used. The database uses a global distribution of soil  
209 parent material and lithological dependent P concentrations along with a pedogenesis  
210 transformation model to simulate the weathering of each parent rock type. The authors present  
211 global distributions of P in different forms as an average of the top 50 cm of the soil profile,  
212 including total-P (TP), labile inorganic P (Lab-P), and apatite-P (Ap-P). A database of global soil  
213 CaCO<sub>3</sub> content was obtained from the gridded Global Soil Dataset for use in Earth System  
214 Models (GSDE) developed by Shangguan et al. (2014). A mean content was determined using  
215 the top 50cm of data in order to provide comparable emissions to the P components and to  
216 maximise global coverage of emissions. Figure 1 shows the datasets regridded to a 2.8°  
217 horizontal resolution. Dust TP content typically ranges from 200 – 1000 ppm by mass (global  
218 mean of 563 ppm), Ap-P from 20 – 300 ppm (164 ppm), and Lab-P from 20 – 100 ppm  
219 (50 ppm), whilst CaCO<sub>3</sub> content, at over two orders of magnitude greater, typically ranges from  
220 1 – 12% (global mean of 3.3%) of the total dust mass. In terms of global means Lab-P constitutes  
221 9% of TP dust content and varies between 5 – 10%, whereas Ap-P constitutes 29% of TP and

222 varies between 5 – 60%; the major deserts show less variability and Ap-P tends to represent  
 223 ~50% of TP. The form of P that represents the majority of remaining TP is occluded-P (not  
 224 shown; spatial distribution apparent from the low values of Ap-P:TP). Experimental observations  
 225 from Stockdale et al. (2016) suggest this form of P is not released through acid dissolution nor  
 226 upon deposition to the ocean surface; it is also much more prevalent in the northern boreal  
 227 regions where dust uplift is less important.

228  
 229 To simulate the emission and deposition of the dust mineralogy, tracers were included in  
 230 GLOMAP alongside dust following previous studies (Atkinson et al., 2013 and Vergara-  
 231 Temprado et al., 2017) using the regrided soil-P and CaCO<sub>3</sub> datasets. For each tracer the  
 232 spatially variable mass fraction of the components from the regrided soil-P and CaCO<sub>3</sub>  
 233 databases were applied to the modelled dust emission at each grid point to produce an associated  
 234 mass. Throughout the simulation, dust is considered a single component with the fractional  
 235 partition between the constituents conserved for all processes, including interaction between two  
 236 dust modes. The simulations produce monthly mean wet and dry mass deposition fluxes (both  
 237 impactation and nucleation scavenging) from each grid point for total dust, TP, Ap-P, Lab-P,  
 238 CaCO<sub>3</sub>, and dust-associated acid in the form of the sulfate component.

239  
 240 The acid dissolution process is simulated using parameterizations based on experimental  
 241 observations from Stockdale et al. (2016), which provide robust evidence that the dissolution of  
 242 Ap-P occurs rapidly (seconds to minutes) and that the system can be replicated by a simple linear  
 243 relationship between acid input and Ap-P / CaCO<sub>3</sub> dissolution. Linear fits to the experimental  
 244 data on a logarithmic scale using all dust samples provides the mass of dissolved Ap-P and  
 245 CaCO<sub>3</sub> as a function of the absolute number of protons available. The dissolution rate of Ap-P  
 246 increases in the absence of CaCO<sub>3</sub>, therefore an additional step has been introduced to simulate  
 247 the enhanced dissolution rate. Stockdale et al. (2016) found that the dissolution of hydroxyapatite  
 248 powder was well reproduced by the geochemical PHREEQC model (Parkhurst and Appelo,  
 249 2013); this model was used to produce a linear fit between available protons and dissolution of  
 250 Ap-P, which provides a means for estimating Ap-P dissolution in the absence of CaCO<sub>3</sub>. The  
 251 resulting parameters from the linear fits can be found in the supporting information (Table S1).  
 252 At each grid point (horizontal and vertical) the number of protons available, determined from the  
 253 mass of dust-associated sulfate and assuming each mole of H<sub>2</sub>SO<sub>4</sub> dissociates to produce 2 moles  
 254 of H<sup>+</sup>, is used to determine the number of moles of deposited dissolved CaCO<sub>3</sub> (mol CaCO<sub>3,diss</sub>)  
 255 using Eq. 1. Applying mol CaCO<sub>3,diss</sub> to Eq. 2 provides dissolved Ap-P (mol Ap-P<sub>diss</sub>) from  
 256 simultaneous dissolution of Ap-P and CaCO<sub>3</sub>. If all CaCO<sub>3</sub> has been dissolved (i.e.,  
 257 mol CaCO<sub>3,diss</sub> = mol CaCO<sub>3,available</sub>) any excess protons are used to determine a second  
 258 source of mol Ap-P<sub>diss</sub> using Eq. 2 under the condition that mol CaCO<sub>3,available</sub> = 0. The  
 259 number of moles of dissolved Ap-P from simultaneous and separate dissolution, constrained by  
 260 the available deposited mass of Ap-P, is integrated over each horizontal grid point to provide a  
 261 monthly mean surface deposition flux of bioavailable P from Ap-P dissolution. The deposition  
 262 fluxes of Lab-P are similarly integrated over each grid point and added to the dissolved Ap-P to  
 263 provide the total atmospheric bioavailable P flux to the surface from inorganic mineral dust.

264

$$\log_{10}(\text{mol CaCO}_{3,\text{diss}}) = a_1 + b_1 \cdot \log_{10}(\text{mol H}^+) \quad (1)$$

265



$$\log_{10}(\text{mol ApP}_{\text{diss}}) = \begin{cases} a_2 + b_2 \cdot \log_{10}(\text{mol CaCO}_3_{\text{diss}}), & \text{if mol CaCO}_3_{\text{available}} > 0 \\ a_3 + b_3 \cdot \log_{10}(\text{mol H}^+_{\text{excess}}), & \text{if mol CaCO}_3_{\text{available}} = 0 \end{cases} \quad (2)$$

266

267 **3 Results**

## 268 3.1 Bioavailable phosphorus

269 Annual deposition fluxes of bioavailable phosphorus (Bio-P) from dust, dust mass, and the dust-  
 270 associated acid for the year 2001 are shown in Figure 2. The large spatial variability in dust  
 271 deposition drives the spatial variability of Bio-P. Highest values are found close to major dust  
 272 source regions of Sahara and Kalahari deserts in Africa, and across central Asia, the Americas,  
 273 and Australia. A significant proportion of the dust is deposited close to the source of emission.  
 274 However, considerable transport occurs from all dust source regions driven by large-scale  
 275 meteorology, most notably the transport of African dust advecting westwards across the Atlantic  
 276 Ocean driven by trade winds, and mid-latitude transport from South America and South Africa  
 277 eastwards. Northern Hemisphere mid-latitude transport from Asia across the western and central  
 278 Pacific Ocean also provides a considerable transport route for dust to these remote ocean regions.  
 279 The amount of acid condensed onto the mineral dust (Figure 2c) shows a strong correlation with  
 280 regions of high pollution and dust transport. The industrialized regions of North America,  
 281 Europe, central and eastern Asia can be clearly identified, as well as regions of biomass burning  
 282 in central Africa. Transported pollutants also play a considerable role over the north-west Pacific  
 283 and North Atlantic, as well as northern Africa and the Mediterranean Sea. The low dust loading  
 284 in the central Pacific and Atlantic coincident with a moderate amount of acid highlights the  
 285 marine source of sulfate emissions from DMS in this region, and a similar correlation in the  
 286 northern high latitudes highlights the transport of pollutants from Europe and North America to  
 287 this remote region.

288  
 289 Table 1 provides a breakdown of absolute mass and mass per unit area deposited per year  
 290 globally, on terrestrial ecosystems, on marine ecosystems, and into each ocean basin and  
 291 continent; boundaries to each basin are shown in the supporting information (Figure S2).  
 292 Globally, 117 Gg-P yr<sup>-1</sup> Bio-P from mineral dust is deposited to the surface annually, with  
 293 86 Gg-P yr<sup>-1</sup> to the continents and 31 Gg-P yr<sup>-1</sup> to the oceans and seas. The large value over land  
 294 is dominated by Africa (52 Gg-P yr<sup>-1</sup>) and Asia (24 Gg-P yr<sup>-1</sup>), both of which contain large areas  
 295 of desert and reflect short-range transport from these important source regions. There is a  
 296 considerable spatial variability over the ocean basins. The North Atlantic, North Pacific, and  
 297 Indian Oceans dominate the absolute mass of Bio-P deposited to the surface waters accounting  
 298 for 37%, 19%, and 18% of all Bio-P deposited to the oceans and seas, respectively. In the North  
 299 Atlantic and Indian Ocean this is correlated with the dust mass deposition (52% and 21%), whilst  
 300 the North Pacific accounts for only 11% of global dust supply to surface waters. This apparent  
 301 enrichment is due to relatively enhanced acid dissolution, which will be discussed in the  
 302 following section. The global importance of the Mediterranean Sea as a region impacted by dust  
 303 is clearly demonstrated; it accounts for 5% of the total ocean Bio-P and results in the largest  
 304 deposited mass per unit area over the oceans (1.5 µg-P m<sup>-2</sup>day<sup>-1</sup>) and is exceeded on land only by  
 305 Africa (4.8 µg-P m<sup>-2</sup>day<sup>-1</sup>) and Asia (1.5 µg-P m<sup>-2</sup>day<sup>-1</sup>), which are both important dust source  
 306 regions. The NE Atlantic is also strongly impacted because of its proximity to the Saharan

307 Desert, which exhibits a strong outflow over this region and results in a mean deposition rate of  
308  $1.2 \mu\text{g-P m}^{-2}\text{day}^{-1}$ .  
309

### 310 3.2 Acid dissolution vs labile P

311 As observed by Stockdale et al. (2016) mineral dust contains Ap-P and Lab-P that both  
312 contribute towards the total fraction of inorganic mineral-borne phosphorus that is potentially  
313 bioavailable in marine surface waters. Although measurements reported by Stockdale et al.  
314 (2016) find Lab-P present in much smaller quantities than Ap-P, the total mass of Lab-P is  
315 directly bioavailable in the surface waters, whereas the Ap-P requires the presence of acid to  
316 yield a bioavailable form of P, hereafter referred to as Acid-P. The differences in immediate  
317 bioavailability of the two components results in distinct regional differences that can be seen in  
318 Figure 3 (panels a and b). Close to the dust source regions (Saharan, Arabian, Gobi, Patagonian,  
319 Kalahari, Great Basin, and Great Australian deserts) the Lab-P dominates the total Bio-P  
320 deposition, whereas further away from source regions and over industrialized regions Acid-P  
321 dominates; the formation of Acid-P is enhanced as dust accumulates condensed acids during  
322 long-range transport and when dust loading is low in proximity to local pollution sources (thus  
323 highlighting areas that are possibly acid-limited in respect to the dissolution of Ap-P). DMS can  
324 also play a role in providing a source of acid over the open oceans, especially in the Pacific  
325 Ocean, Southern Ocean, and Arctic Ocean (Belviso et al., 2004).  
326

327 Table 1 and Table 2 provide regional information on the annual mean contribution from Lab-P  
328 and Acid-P. Of the total  $31.2 \text{ Gg-P yr}^{-1}$  of Bio-P deposited to the oceans  $16.9 \text{ Gg-P yr}^{-1}$  is from  
329 Acid-P and  $14.3 \text{ Gg P yr}^{-1}$  from Lab-P. The North Atlantic Ocean, Mediterranean Sea, and the  
330 western Indian Ocean, all regions strongly influenced by their proximity to significant dust  
331 sources, are dominated by the Lab-P fraction with 94% of the ocean's total Lab-P mass being  
332 deposited in these three regions (73%, 7%, and 14%, respectively). Conversely, the Pacific  
333 Ocean, Arctic Ocean, SE Atlantic, South China Sea, and the Southern Ocean, regions further  
334 from dust source regions, are dominated by the acid dissolution process; in these regions the  
335 contribution of Acid-P to the total Bio-P ranges from 75% to 81%. Although dominated by Lab-  
336 P the North Atlantic Ocean, Mediterranean Sea, and western Indian Ocean also receive a  
337 considerable mass of Bio-P from Acid-P. Considerable acid dissolution of Ap-P occurs over the  
338 Pacific Ocean even though this region receives a very small mass of dust (14% of global oceans  
339 dust supply, 25% of global oceans Bio-P supply).  
340

### 341 3.3 Spatial variability of TP bioavailability

342 Estimated percentages of TP bioavailability for dust are shown in Figure 3c and Table 2. The  
343 simulated TP bioavailability from dust varies from ~10% to 60% and is generally negatively  
344 correlated with areas of high dust loading, and positively correlated with acid loading. The Lab-P  
345 content in dust tends to only vary between 9% and 11% of the TP across the globe (see Table 2).  
346 As this pool of phosphorus is deemed directly bioavailable, Bio-P in regions of high dust loading  
347 will be dominated by the Lab-P component and are likely to be less dependent on changes to  
348 acid concentrations. The dominance of Lab-P in high dust loading regions can be seen close to  
349 dust source regions over land and in the NE Atlantic Ocean where TP bioavailability (14%) is  
350 closely matched with the content of Lab-P in the dust (10%). Conversely, in regions that are not

351 dominated by dust loading, such as the central Pacific and the remote Arctic Ocean, Acid-P has a  
352 greater impact and results in a greater TP bioavailability (~50%). Due to the almost constant  
353 percentage of Lab-P in dust TP content the variability in TP bioavailability across the globe is  
354 controlled by the acid dissolution process; this is apparent from the wide range in percentage  
355 contribution of Acid-P in Table 2, which ranges from only 7% over Africa and 29% over the NE  
356 Atlantic, to over 77% in the Pacific and 81% over the Arctic Ocean. These findings highlight the  
357 importance that acid dissolution has on the deposition of Bio-P from dust to remote regions that  
358 have fewer sources of nutrients, such as the Greenland and Antarctic ice sheets, and the Arctic  
359 and Southern oceans. These estimates only refer to the bioavailability of dust-borne P. Results  
360 from the modelling study of Myriokefalitakis et al. (2016) suggest dust is the dominant driver of  
361 the collective bioavailability of P-containing aerosol species in northern hemisphere oceans,  
362 whereas in the southern hemisphere primary biological particles are more pronounced in the  
363 South Atlantic and South Pacific Oceans, and sea spray in the Southern Ocean. Therefore, our  
364 estimates are likely representative of northern hemisphere oceans, but other sources of P may  
365 increasingly drive the observed bioavailability in the high southern hemisphere latitudes.  
366

#### 367 3.4 Sensitivity of acid dissolution to degree of particle external mixing

368 The assumption used in this study is that a given mass of dust particles can be treated as if they  
369 are internally mixed, with each dust constituent (Ap-P, Lab-P, and  $\text{CaCO}_3$ ) being present at a  
370 constant fraction of each particle's mass, i.e., in each grid box every particle will contain the  
371 same mass fraction of Ap-P, Lab-P, and  $\text{CaCO}_3$ . This is not necessarily important for the Lab-P  
372 fraction, but the dissolution of Ap-P into Acid-P occurs simultaneously with the dissolution of  
373  $\text{CaCO}_3$  at a rate that is faster than when no  $\text{CaCO}_3$  is present.  
374

375 To understand the importance of the particle mixing assumption, the deposited masses of dust  
376 and associated acid were split into distinct components to mimic a population of internally and  
377 externally mixed particles of varying concentrations. As previously, all Lab-P is deemed  
378 bioavailable, and hence the deposited Lab-P mass is the same as in the previous experiments. For  
379 a given percentage of externally mixed particles the relevant percentage mass of Ap-P is treated  
380 separately using Eq. 2 and assuming no  $\text{CaCO}_3$  present, whilst the remaining mass of Ap-P is  
381 assumed internally mixed and treated as per the control experiment using Eq. 2 with the  
382 corresponding mass of  $\text{CaCO}_3$ . A third group, consisting of the externally mixed  $\text{CaCO}_3$  is also  
383 removed but has no direct impact on the Bio-P and is simply removed along with its associated  
384 condensed acid (thereby having an indirect effect on Bio-P). The modelled uptake efficiency of  
385 acid onto the mineral particle is independent of the degree of external mixing. The total Bio-P  
386 deposited is the sum of Lab-P, internally mixed Acid-P, and externally mixed Acid-P. Externally  
387 mixed percentages of 1%, 2%, 5%, 10%, 25%, 50%, and an extreme case of 100% were used to  
388 determine the change in total Bio-P deposition to each region as a percentage of the control  
389 experiment where all particles are assumed to be internally mixed (0% externally mixed). Results  
390 are shown in Table 3.  
391

392 The results show that the Bio-P deposition is very sensitive to the assumptions used for the  
393 distribution of components between dust particles. All regions show an increasing deposition rate  
394 of Bio-P with an increasing degree of external mixing. An increase from 0% to 5% results in a  
395 9% increase of Bio-P to the oceans, with most of this from regions with large dust loadings

396 where acid dissolution of Ap-P is usually strongly buffered by CaCO<sub>3</sub>. Regions that show less  
397 sensitivity are those where acid dissolution is already a dominating process and CaCO<sub>3</sub> is close  
398 to exhaustion; in this case the enhanced dissolution rate of Ap-P is already occurring. In reality it  
399 is unlikely that CaCO<sub>3</sub> and Ap-P will be exclusively present on different particles, but this  
400 provides insight of how sensitive the process is, and clearly suggests that this assumption is  
401 important for determining the dissolution process of Ap-P, and also other minerals that would  
402 usually be buffered by the CaCO<sub>3</sub>.

403

### 404 3.5 Evaluation of model simulation

405 Our modelled deposition fluxes, solely from mineral dust, are evaluated against a dataset of  
406 observed fluxes and in-situ aerosol concentrations from ocean cruises and ground-based  
407 observations compiled by Vet et al. (2014) which includes data from a number of sources (Baker  
408 et al., 2006a; Baker et al., 2006b; Baker et al., 2010; Carbo et al., 2005; Chen and Chen, 2008;  
409 Chen, 2004; Furutani et al., 2010; Herut et al., 1999; Kocak et al., 2005; Koelliker et al., 2004;  
410 Markaki et al., 2003; Migon and Sandroni, 1999; Morales-Baquero et al., 2006;  
411 NADP/AIRMoN, 2010; Oredalen et al., 2010; Ozsoy, 2003; Rodríguez et al., 2011; Tamatamah  
412 et al., 2005; Zhang et al., 2007). Figure 4 and Figure 5a show the observations compared to the  
413 modelled deposition fluxes from our study. Although limited by observations, the model captures  
414 the regional variations in TP: the highest values are found close to source regions, such as the  
415 Mediterranean Sea and off the eastern coast of Africa, and lower values in more remote regions,  
416 such as the central Pacific. Apparently linear features in Figure 5a for the Pacific coast and  
417 Mediterranean occur due to multiple observations being present in the same model grid-box.  
418 Standard deviations of model data, shown in Figure 5a, show considerable variability throughout  
419 the year. The observational dataset contains P from all sources, whereas we only estimate fluxes  
420 for mineral dust. The results support the idea that mineral dust is a globally important source of  
421 P, but it is worth noting that in regions of low dust loading, such as the Southeast Pacific and  
422 Southern Ocean, other sources of P may play a more important role (Myriokefalitakis et al.,  
423 2016).

424

425 We also compared our Bio-P estimates to field observations in Figure 4 and Figure 5b. The  
426 model reproduces the observations within an order magnitude for much of the Atlantic Ocean  
427 and Mediterranean Sea but, as with TP, is under-estimating values over the Pacific Ocean and  
428 the land; the under-representation over land is likely due to the enhanced role of other sources of  
429 P. A key result is that when acid dissolution is removed from the model, shown in Figure 5b  
430 using crossed symbols, the Bio-P values are systematically too low compared with  
431 measurements. The normalized mean bias (and with respect to the logarithm) without acid  
432 dissolution is -0.60 (-0.27) and -0.54 (-0.1) when acid dissolution is included. Our model  
433 confirms that acid dissolution in the atmosphere is an important process affecting the deposited  
434 flux of Bio-P (through the addition of Acid-P) to the Earth's surface.

435

436 Overall TP deposition fluxes to ocean basins and seas are compared to other modelling studies in  
437 Table 4. Regional trends show good agreement with other studies: The North Atlantic Ocean is  
438 the globally dominant region for deposition, with the North Pacific Ocean and Indian Ocean also  
439 important regions for deposition. Our results show good agreement with Zhang et al. (2013),  
440 who similarly only considered mineral dust, in all regions except for the North Atlantic for which

441 the authors estimate an additional 40% deposition of TP. Okin et al. (2011) and Myriokefalitakis  
442 et al. (2016) estimate similar fluxes for the Atlantic Ocean but estimate a factor of ~2 to 3 greater  
443 deposition to the Pacific and Indian oceans. Mahowald et al. (2008) estimate considerably  
444 greater fluxes in most regions: the Atlantic Ocean is a factor of 3 greater, and the Pacific and  
445 Indian oceans are a factor of ~4 greater than our estimates. These differences are largely due to  
446 the assumed P content of dust. In our study the P content of the emitted dust was determined  
447 using a soil P-content database from Yang et al. (2013), which results in a global mean TP  
448 content of 489 ppm per mass of dust. Mahowald et al. (2008), assumed a constant P content of  
449 720 ppm, Okin et al. (2011) use 700 ppm, whilst Myriokefalitakis et al. (2016) use a soil  
450 database (Nickovic et al., 2012) and tune emissions to result in a global mean dust TP content of  
451 880 ppm. Using these alternative global mean contents and our modelled dust fluxes would  
452 result in equivalent ocean TP deposition fluxes of 212, 206, and 259 Gg-P yr<sup>-1</sup>.  
453

454 Table 4 also compares Bio-P from this study with other modelling studies. Zhang et al. (2015)  
455 provide a good comparison as their study only considers inorganic P from dust and uses a  
456 globally constant TP bioavailability for each mineral, experimentally determined in solution with  
457 a pH of 2. In contrast we use a parameterization based on experiments using a full range of  
458 conditions, which results in a TP bioavailability that depends on acidity levels and dust loading.  
459 In Zhang et al. (2015) the TP bioavailability is ~10% for most of the basins, whereas in this  
460 study the bioavailability varies from ~15% in areas of high dust loading to > 45% in regions of  
461 high pollution or remote regions only accessible through long-range transport. This results in a  
462 global deposition of Bio-P in our study (31.2 Gg-P yr<sup>-1</sup>) that is roughly double that of Zhang et  
463 al. (2015). Mahowald et al. (2008) estimate Bio-P ocean deposition of 96.5 Gg-P yr<sup>-1</sup>, which is  
464 roughly three times our estimate. In their study a constant TP bioavailability of 10% for mineral  
465 dust is used. However, the inclusion of other P sources results in a TP bioavailability from all P  
466 sources that is greater than 10% in regions where other P sources are important, such as the  
467 Pacific and Arctic. The increased TP from other sources, and from the assumed TP content of  
468 dust, results in a greater Bio-P deposition estimate than our study.  
469

470 Myriokefalitakis et al. (2016) estimate 88.7 Gg-P yr<sup>-1</sup> Bio-P from inorganic sources only (dust-  
471 borne Lab-P, dissolved Ap-P, and volcanic aerosols), which is a factor of ~3 greater than our  
472 study; this difference arises mainly through differences in the TP content of dust, as well as a  
473 different modelled acid dissolution process, and through contributions from volcanic aerosols  
474 (6 Gg-P yr<sup>-1</sup> predominantly to the Pacific Ocean). If we apply the higher dust TP and Lab-P  
475 content from Myriokefalitakis et al. (2016), it increases our global Bio-P estimate by  
476 16 Gg-P yr<sup>-1</sup>. The final difference occurs through the treatment of the Acid-P production; we  
477 estimate 30 Gg-P yr<sup>-1</sup> is deposited globally as Acid-P, compared to 144 Gg-P yr<sup>-1</sup> by  
478 Myriokefalitakis et al. (2016). Part of this difference in Acid-P is due to the assumption used in  
479 Myriokefalitakis et al. (2016) that the TP content of dust is comprised of Lab-P and Ap-P only,  
480 whereas other constituents are included in our soil database (e.g., Lab-P and Ap-P make up  
481 ~50% of TP in the Sahara Desert). Assuming our deposited dust is only comprised of Lab-P and  
482 Ap-P would provide a factor 3 increase in Ap-P availability, which as shown by our sensitivity  
483 study (Table S2) could have a considerable impact on Bio-P deposition. The final differences in  
484 Acid-P production occur in the different representations of acid dissolution: in our study the  
485 empirically parameterized process is dependent on the absolute number of H<sup>+</sup> ions from H<sub>2</sub>SO<sub>4</sub>  
486 and HNO<sub>3</sub> uptake and calculated offline after deposition, whereas in Myriokefalitakis et al.

487 (2016) an online aerosol thermodynamic equilibrium framework is used to determine conditions  
488 for use in a kinetic model. The added sources of atmospheric acid and detailed treatment of the  
489 particle's aqueous composition results in greater acid dissolution than the simple experimentally  
490 based method used in our study. However, despite these differences it is an interesting result that  
491 the two methods produce similar spatial patterns but of different magnitudes. Assessing these  
492 differences and identifying the more appropriate method are beyond the scope of this study but  
493 merit further attention.  
494

#### 495 **4 Discussion**

496 There is large spatial variability in the amount of Bio-P supplied to the surface ocean. The largest  
497 flux of dust and of Bio-P, predominantly in the form of Lab-P, is supplied to the NE Atlantic  
498 Ocean; this area is known to have a high dust flux from the world's major source of mineral dust,  
499 the Sahara Desert. The modelling suggests that this area not only has the highest total input of  
500 Bio-P ( $6.9 \text{ Gg-P yr}^{-1}$ ) but also a high input of Bio-P per unit area ( $436 \mu\text{g-P m}^{-2}\text{yr}^{-1}$ ; second to the  
501 Mediterranean Sea with  $549 \mu\text{g-P m}^{-2}\text{yr}^{-1}$ ). Neuer et al. (2004) suggest the pulses of Saharan dust  
502 seem to exert a feast or famine effect on phytoplankton export from this region. A pulsing that  
503 may be linked to the observed phytoplankton export is apparent in the modelled fluxes (Figures  
504 S3 to S6) which vary between 0.2 and 0.6 Gg-P per month in the NE Atlantic and between 0.4  
505 and 0.9 Gg-P per month in the NW Atlantic, another region with considerable deposition of Bio-  
506 P. In these regions, Saharan dust plumes transported over the N Atlantic meet N American air  
507 masses which are enriched in anthropogenic combustion products. Sedwick et al. (2007)  
508 identified an increase in soluble Fe delivered to the offshore NW Atlantic caused by the N  
509 American polluted air masses. Here we show based on our modelling that these air masses also  
510 increase the amount of Acid-P from the mineral dust transported across the Atlantic from the  
511 Sahara, especially during the summer months when dust transport and acid pollution are both  
512 relatively enhanced.  
513

514 The total Bio-P supplied to the ocean is the sum of contributions from Lab-P and Acid-P. The  
515 location with the highest mass of deposited Bio-P from Acid-P is the NW Pacific ( $3.6 \text{ Gg-P yr}^{-1}$ ).  
516 Our data (Table 1) is averaged over the whole NW Pacific area, however the impact is greatest in  
517 the area directly under the plume from the Gobi and Taklamakan deserts which passes over the  
518 highly polluted air in East Asia (Jaffe et al., 1999) and out into the NW Pacific (Chen et al.,  
519 2017). This plume is rather narrowly confined to  $\sim 40^\circ\text{N}$  but has a large effect within that plume  
520 as shown in Figures S3 and S4. We see the strongest peak during the Northern Hemisphere  
521 spring (March-April-May; Figure S5), which is consistent with the findings of Chen et al.  
522 (2017). Maki et al. (2016) find that Asian dust is a major nutrient source to the area of the NW  
523 Pacific under the plume though their study concentrates on the flux of atmospheric nitrate to this  
524 N limited region. As argued below the greatly increased flux of Bio-P from the dust plume will  
525 reduce the potential effect of switching to P limitation and may also increase the  $\text{N}_2$  fixation in  
526 the surface waters (Jickells and Moore, 2015) as well as increasing the total primary productivity  
527 over longer timescales (Tyrell, 1999).  
528

529 The location with the highest annual mass of Bio-P per unit area ( $\sim 550 \mu\text{g-P m}^{-2}\text{yr}^{-1}$ ) is the  
530 Mediterranean Sea. This area is particularly sensitive to the addition of extra Bio-P since both the  
531 Western and particularly the Eastern Mediterranean are P limited (Krom et al., 1991; Moutin and

532 Raimbault, 2002; Powley et al., 2017). Any addition of P available to the phytoplankton will  
533 rapidly be taken up into the P-starved water (Krom et al., 2005) and be translated into extra  
534 primary productivity. Microcosm experiments have shown the importance of dust inputs to  
535 increasing primary productivity particularly during the summer when there is minimal nutrient  
536 supply from below (Laghdass et al., 2012; Ridame et al., 2014). Krom et al. (2010) estimated  
537 that Lab-P from atmospheric sources provided 30% of the non-marine external P supplied to the  
538 Eastern Mediterranean while Powley et al. (2017), using a mass-balance model, estimated that  
539 49% of the non-marine external supply to the entire Mediterranean was from atmospheric  
540 supply. African dust outbreaks are estimated by Pey et al. (2013) to occur over the  
541 Mediterranean over 20% of annual days. These plumes of mineral dust, along with locally  
542 derived sources, meet air polluted with acidic gases from Europe including air that has passed  
543 over cities such as Athens (Nenes et al., 2011); this results in extra Acid-P, and thus Bio-P, being  
544 produced. The modelling results are compatible with the predictions made by Nenes et al. (2011)  
545 concerning the effect of acid processing on mineral aerosol over the Mediterranean.  
546

547 There is also a considerable contribution from Acid-P in both the western and eastern Indian  
548 Ocean. This is an area where dust from local desert regions such as the Arabian Peninsula and  
549 the Thar desert in India meet with air masses polluted from highly populated areas in South and  
550 South-East Asia (Lelieveld et al., 2001), and pollution from biomass burning over Central and  
551 South-eastern Africa and South Asia (Sinha et al., 2004). It has been suggested that atmospheric  
552 aerosols including dust particles, as well as biomass burning and other anthropogenic sources,  
553 are increasing the flux of dissolved nutrients (including phosphate) to the Bay of Bengal  
554 (Srinivas and Sarin, 2015). Rengarajan and Sarin (2004) suggested that aerosols that have been  
555 involved in interactions between mineral dust and pollution also impacted the Arabian Sea; they  
556 identified its effect on Fe and NO<sub>x</sub>. Here we suggest it also affects the Acid-P.  
557

558 It is generally assumed that any potential Bio-P (i.e., mineral apatite and/or Fe-bound P) as well  
559 as Lab-P that lands on most parts of the terrestrial system will be consumed by plants. Plants and  
560 their accompanying mycorrhizal fungi are evolved to extract this key nutrient from such minerals  
561 present in the soil (Smits et al., 2012). The only exception to this might be areas of snow, such as  
562 Greenland and the Arctic, which host algal communities which are important for climate change  
563 due to their impact on surface albedo (Lutz et al., 2016). It has been reported that microbes in  
564 arctic glaciers live in P-deficient environments (Stibal et al., 2009) which suggests that  
565 atmospheric input of Bio-P to these key regions may play an important role on local algal and  
566 microbial activity. We estimate that the amount of Bio-P delivered to the major ice sheets of the  
567 world (Greenland and Antarctica) is 0.08 Gg-P yr<sup>-1</sup> of which the majority (~80%) is produced by  
568 acid dissolution.  
569

570 Modelling studies routinely use a constant value for TP bioavailability, which typically ranges  
571 from ~10 to ~15%. From the soil P database used in our study we show that TP bioavailability is  
572 at least 10% due to Lab-P alone and is considerably greater once the Acid-P contribution is  
573 included. For inorganic Bio-P from mineral dust we estimate global mean TP bioavailability of  
574 22% and 12% for oceans and land, respectively. For the ocean basins, we estimate the following:  
575 Pacific Ocean (425%); Atlantic Ocean (18%); Indian Ocean (20%); Mediterranean (15%);  
576 Southern Ocean (46%); and Arctic Ocean (55%). Other studies such as Myriokefalitakis et al.  
577 (2016) show similar increases in TP bioavailability caused by Acid-P. These calculations suggest

578 that while the spatial variability of TP and Bio-P are similar (Table 4), the absolute fluxes vary  
579 considerably to a large extent because of different values for TP in the source material.  
580 Uncertainties in current soil databases primarily arise from a lack of observations and sampling  
581 of under-represented soil types, including species that contain phosphorus (Nickovic et al., 2012;  
582 Yang et al., 2013); the result is poor spatial coverage and a lack of process-level understanding  
583 that yields considerable uncertainties. The sensitivity experiments (Table 3 and Table S2)  
584 highlight the clear need for improved estimates of dust-borne P components at source.

585  
586 Krishnamurthy et al. (2010) calculated that the addition of atmospheric P to the global ocean will  
587 increase the total carbon uptake by 0.12% based on an estimated 8.3 Gg-P yr<sup>-1</sup> Bio-P deposited to  
588 the oceans. However, the authors assumed a globally constant dust TP content of 1050 ppm and  
589 a globally constant TP bioavailability of 15%. In comparison our model estimates Bio-P  
590 deposition from inorganic mineral dust to be ~400% of this value (31.2 Gg-P yr<sup>-1</sup>) with TP  
591 bioavailability ranging from ~15% to ~50%. Our enhanced Bio-P deposition estimate suggests  
592 the total carbon uptake could be even greater, if the apatite and CaCO<sub>3</sub> composition in the  
593 mineral dust population were externally mixed. Assuming all Bio-P is taken up by  
594 phytoplankton, and applying the Redfield ratio, our results suggest the atmospheric input of Bio-  
595 P from mineral dust may account for an uptake of 1.3 Tg-C yr<sup>-1</sup>, with 0.7 Tg-C yr<sup>-1</sup> from acid-  
596 dissolution of mineral dust. If the mineral dust Ap-P/CaCO<sub>3</sub> content is deemed 100% externally  
597 mixed, then the total uptake would be 3.0 Tg-C yr<sup>-1</sup>.

598  
599 In non Fe-limited areas where the system is N limited in the short term, it has been shown that  
600 most atmospheric input has a high bioavailable N:P ratio and an excess of Fe. It has been  
601 suggested that the input of Fe and N causes the systems to switch towards P limitation (Jickells  
602 and Moore, 2015). The increased Bio-P shown to be formed by these atmospheric acid processes  
603 linked mainly to anthropogenic pollution will slow this process down particularly in areas like  
604 the NW Atlantic (Chien et al., 2016). This study suggests that the abundant acid gases produced  
605 during volcanic eruptions are likely to have a short term but possibly dramatic effect on the  
606 supply of Bio-P to the ocean. Previous work has been confined to the actual Bio-P produced  
607 within the volcanic plume itself, which is rather small (e.g., Mahowald et al., 2008). Here we  
608 predict that a more important effect might be to increase the flux of Bio-P to the ocean due to the  
609 interaction of acid gasses from the volcano with existing mineral particles in the atmosphere.

610  
611 Stoichiometric proxies have been used to estimate nitrogen fixation rates in oceanic surface  
612 waters. Deutsch et al., (2007) calculated a parameter ( $P^* = PO_4^{3-} - NO_3^-/16$ ) and suggested that  
613 regions with high P\* are also regions of the ocean with high N<sub>2</sub> fixation rates and vice versa. It is  
614 noticeable that the three regions of the global ocean with low values of P\* in their calculations  
615 (north central Atlantic, north western Pacific, and Mediterranean) are also the areas with the  
616 predicted highest fluxes of Acid-P. Superficially the addition of extra bio-P should increase P\*,  
617 however a large fraction of the acid which produces acid-P is nitric acid. This is apparent in the  
618 Eastern Mediterranean where the Atmospheric N:P ratio has been observed as high as 105:1  
619 (Markaki et al., 2010). This is an area of the ocean with very low N<sub>2</sub> fixation rates (Yogev et al.,  
620 2011). By contrast the N<sub>2</sub> fixation rate of the north central Atlantic is relatively high because the  
621 high flux of Saharan dust contains abundant Fe and P, which are required by N<sub>2</sub> fixing organisms  
622 (Mills et al., 2004). It is unclear what overall impact the external supply of bio-P from mineral



623 dust has on N<sub>2</sub> fixation rates and P\*, however, our results provide global estimates that may help  
624 to improve our understanding in the future.

## 625 **5 Summary**

626 In this study a parameterization for acid-dissolution of mineral apatite, developed using results  
627 presented by Stockdale et al. (2016), was incorporated into a global aerosol model (GLOMAP;  
628 Mann et al., 2010) with a global soil P database (Yang et al., 2013) to model the atmospheric  
629 flux of inorganic bioavailable P from mineral dust. We estimate that 870 G-P yr<sup>-1</sup> of inorganic  
630 TP associated with dust is deposited globally, with 726 Gg-P yr<sup>-1</sup> to the land and 144 Gg-P yr<sup>-1</sup> to  
631 the oceans. Our model is able to discriminate between the leachable (labile) pool of phosphorus  
632 which is present upon emission and the dissolved apatite pool which is a result of the  
633 simultaneous acid-dissolution of apatite and calcium-carbonate; the two pools combined  
634 represent the atmospheric flux of bioavailable phosphorus from dust.

635  
636 We estimate a global flux of 31 Gg-P yr<sup>-1</sup> Bio-P to the oceans with 14.3 Gg-P yr<sup>-1</sup> from the labile  
637 pool (Lab-P), and 16.9 Gg-P yr<sup>-1</sup> from the acid-dissolved pool (Acid-P). The acid dissolution of  
638 mineral dust increases supply of Bio-P to the oceans by 120%, showing the importance of the  
639 acid dissolution process on global Bio-P fluxes. We identify the Mediterranean Sea, North  
640 Atlantic Ocean, and North Pacific Ocean as particularly important regions for dust-borne Bio-P  
641 deposition.

642  
643 Our modelling results show that the percentage of deposited dust TP that is in a bioavailable  
644 form ranges from ~10% to ~50%, however, generally it has been assumed in modelling studies  
645 that the percentage of mineral dust TP bioavailability is globally constant, with values between  
646 10% and 15% commonly used. We use a similar approach to Myriokefalitakis et al. (2016) to  
647 show that although the labile fraction of TP is globally constant at ~10%, the acid-dissolved pool  
648 increased the mean TP bioavailability over oceans to 22% with considerable variation between  
649 ocean basins: Pacific Ocean (45%); Atlantic Ocean (23%); Indian Ocean (21%); and  
650 Mediterranean (15%). This variability again highlights the impact that the acid-dissolution  
651 process has on the global flux of Bio-P from dust.

652  
653 The world's largest dust sources all have relatively enriched levels of dust-P pools but show  
654 variability between sources. We therefore advise against using global constant values for dust-P  
655 pools and recommend using global databases of soil-P content. In our study we used a  
656 pedogenesis-based soil-P database from Yang et al. (2013) which resulted in a global mean  
657 deposited dust TP content of 489 ppm with 49 ppm from Lab-P and 243 ppm from Ap-P, with all  
658 pools displaying roughly one order of magnitude variability across the globe. Comparing these  
659 results with other modelling studies and results from a series of sensitivity tests highlighted the  
660 affect that the assumed dust mineralogical content has on the Bio-P flux. It is noted that there is  
661 no consensus on the global mean deposited dust TP and previous studies have used higher values  
662 (e.g., 880 ppm by Myriokefalitakis et al. (2016) and 720 ppm by Mahowald et al. (2008)).  
663 From our sensitivity study we have identified that treating the dust population as an externally  
664 rather than internally mixed population (i.e., assuming the population exhibits particle-to-particle  
665 diversity in apatite and CaCO<sub>3</sub> content) results in a considerable increase in global Bio-P flux  
666 (44% increase for a 25% externally mixed population). It is currently not known which treatment  
667 is appropriate and requires more research.

668  
669 Our results confirm the importance of acid processes in the atmosphere in increasing the flux of  
670 Bio-P to the global ocean as suggested by Nenes et al. (2011). The effect is spatially and  
671 temporally variable and it is suggested that increased Bio-P can result in regionally important  
672 changes in biogeochemical processes such as nutrient limitation, nitrogen fixation rates and  
673 carbon uptake.  
674

#### 675 **Acknowledgements**

676 This research was funded by the Leverhulme Trust Research Project Grant RPG 406, entitled  
677 “Understanding the Delivery of phosphorus nutrient to the oceans”. KSC acknowledges funding  
678 from the EU CRESCENDO project under grant agreement No 641816. The authors wish to  
679 thank T. Nenes, M. Kanikidou, and S. Myriokefalitakis for useful discussions and for providing  
680 data used in the comparison to Myriokefalitakis et al. (2016). The authors also wish to thank R.  
681 Vet for providing the observational dataset used; this source is listed in the references. Other data  
682 used are listed in the references, tables, and supplementary information.  
683

#### 684 **References**

- 685 Atkinson, J. D., Murray, B. J., Woodhouse, M. T., Whale, T. F., Baustian, K. J., Carslaw, K. S.,  
686 Dobbie, S., O'Sullivan, D., and Malkin, T. L. (2013), The importance of feldspar for ice  
687 nucleation by mineral dust in mixed-phase clouds. *Nature*, 498, 355-358. 10.1038/nature12278  
688
- 689 Baker, A. R., French, M., and Linge, K. L. (2006a), Trends in aerosol nutrient solubility along a  
690 west–east transect of the Saharan dust plume. *Geophysical Research Letters*, 33, L07805.  
691 10.1029/2005gl024764  
692
- 693 Baker, A. R., Jickells, T. D., Witt, M., and Linge, K. L. (2006b), Trends in the solubility of iron,  
694 aluminium, manganese and phosphorus in aerosol collected over the Atlantic Ocean. *Marine*  
695 *Chemistry*, 98, 43-58. 10.1016/j.marchem.2005.06.004  
696
- 697 Baker, A. R., Lesworth, T., Adams, C., Jickells, T. D., and Ganzeveld, L. (2010), Estimation of  
698 atmospheric nutrient inputs to the Atlantic Ocean from 50°N to 50°S based on large-scale field  
699 sampling: Fixed nitrogen and dry deposition of phosphorus. *Global Biogeochemical Cycles*, 24,  
700 GB3006. 10.1029/2009gb003634  
701
- 702 Belviso, S., Moulin, C., Bopp, L., and Stefels, J. (2004), Assessment of a global climatology of  
703 oceanic dimethylsulfide (DMS) concentrations based on SeaWiFS imagery (1998-2001).  
704 *Canadian Journal of Fisheries and Aquatic Sciences*, 61, 804-816. 10.1139/f04-001  
705
- 706 Brahney, J., Mahowald, N., Ward, D. S., Ballantyne, A. P., and Neff, J. C. (2015), Is atmospheric  
707 phosphorus pollution altering global alpine Lake stoichiometry? *Global Biogeochemical Cycles*,  
708 29, 1369-1383. 10.1002/2015gb005137  
709

- 710 Browse, J., Carslaw, K. S., Arnold, S. R., Pringle, K., and Boucher, O. (2012), The scavenging  
711 processes controlling the seasonal cycle in Arctic sulfate and black carbon aerosol. *Atmospheric*  
712 *Chemistry and Physics*, 12, 6775-6798. 10.5194/acp-12-6775-2012  
713
- 714 Carbo, P., Krom, M. D., Homoky, W. B., Benning, L. G., and Herut, B. (2005), Impact of  
715 atmospheric deposition on N and P geochemistry in the southeastern Levantine basin. *Deep Sea*  
716 *Research Part II: Topical Studies in Oceanography*, 52, 3041-3053. 10.1016/j.dsr2.2005.08.014  
717
- 718 Chen, H.-Y., & Chen, L.-D. (2008), Importance of anthropogenic inputs and continental-derived  
719 dust for the distribution and flux of water-soluble nitrogen and phosphorus species in aerosol  
720 within the atmosphere over the East China Sea. *Journal of Geophysical Research*, 113, D11303.  
721 10.1029/2007jd009491  
722
- 723 Chen, S., Huang, J., Kang, L., Wang, H., Ma, X., He, Y., Yuan, T., Yang, B., Huang, Z., and  
724 Zhang, G. (2017), Emission, transport, and radiative effects of mineral dust from the Taklimakan  
725 and Gobi deserts: comparison of measurements and model results. *Atmospheric Chemistry and*  
726 *Physics*, 17, 2401-2421. 10.5194/acp-17-2401-2017  
727
- 728 Chen, Y. (2004), Sources and Fate of Atmospheric Nutrients over the Remote Oceans and Their  
729 Role on Controlling Marine Diazotrophic Microorganisms, Ph.D. diss., Univ. of Maryland,  
730 College Park.  
731
- 732 Chien, C.-T., Mackey, K. R. M., Dutkiewicz, S., Mahowald, N. M., Prospero, J. M., and Paytan,  
733 A. (2016), Effects of African dust deposition on phytoplankton in the western tropical Atlantic  
734 Ocean off Barbados. *Global Biogeochemical Cycles*, 30, 716-734. 10.1002/2015gb005334  
735
- 736 Chipperfield, M. P. (2006), New version of the TOMCAT/SLIMCAT off-line chemical transport  
737 model: Intercomparison of stratospheric tracer experiments. *Quarterly Journal of the Royal*  
738 *Meteorological Society*, 132, 1179-1203. 10.1256/qj.05.51  
739
- 740 Dentener, F., Kinne, S., Bond, T., Boucher, O., Cofala, J., Generoso, S., Ginoux, P., Gong, S.,  
741 Hoelzemann, J. J., Ito, A., Marelli, L., Penner, J. E., Putaud, J. P., Textor, C., Schulz, M., van der  
742 Werf, G. R., and Wilson, J. (2006), Emissions of primary aerosol and precursor gases in the  
743 years 2000 and 1750 prescribed data-sets for AeroCom. *Atmospheric Chemistry and Physics*, 6,  
744 4321-4344. 10.5194/acp-6-4321-2006  
745
- 746 Deutsch, C., Sarmiento, J. L., Sigman, D. M., Gruber, N., Dunne, J. P. (2007), Spatial coupling  
747 of nitrogen inputs and losses in the ocean. *Nature*, 445, 163-167. 10.1038/nature05392  
748
- 749 Diehl, T., Heil, A., Chin, M., Pan, X., Streets, D., Schultz, M., and Kinne, S. (2012),  
750 Anthropogenic, biomass burning, and volcanic emissions of black carbon, organic carbon, and  
751 SO<sub>2</sub> from 1980 to 2010 for hindcast model experiments. *Atmospheric Chemistry and Physics*  
752 *Discussions*, 12, 24895-24954. 10.5194/acpd-12-24895-2012  
753

- 754 Eijsink, L. M., Krom, M. D., and Herut, B. (2000), Speciation and burial flux of phosphorus in  
755 the surface sediments of the eastern Mediterranean. *American Journal of Science*, 300, 483-503.  
756 10.2475/ajs.300.6.483  
757
- 758 Fuchs, N. A., and Sutugin, A. G. (1971), High-Dispersed Aerosols, in: Topics in Current Aerosol  
759 Research, edited by: Brock, J. R., Pergamon, 1.  
760
- 761 Furutani, H., Meguro, A., Iguchi, H., and Uematsu, M. (2010), Geographical distribution and  
762 sources of phosphorus in atmospheric aerosol over the North Pacific Ocean. *Geophysical*  
763 *Research Letters*, 37, L03805. 10.1029/2009gl041367  
764
- 765 Graham, W. F., and Duce, R. A. (1967), The atmospheric transport of phosphorus to the western  
766 North Atlantic. *Atmospheric Environment*, 16, 1089-1097. 10.1016/0004-6981(82)90198-6  
767
- 768 Herut, B., Krom, M. D., Pan, G., and Mortimer, R. (1999), Atmospheric input of nitrogen and  
769 phosphorus to the Southeast Mediterranean: Sources, fluxes, and possible impact. *Limnology and*  
770 *Oceanography*, 44, 1683-1692. 10.4319/lo.1999.44.7.1683  
771
- 772 Herut, B., Zohary, T., Krom, M. D., Mantoura, R. F. C., Pitta, P., Psarra, S., Rassoulzadegan, F.,  
773 Tanaka, T., and Frede Thingstad, T. (2005), Response of East Mediterranean surface water to  
774 Saharan dust: On-board microcosm experiment and field observations. *Deep Sea Research Part*  
775 *II: Topical Studies in Oceanography*, 52, 3024-3040. 10.1016/j.dsr2.2005.09.003  
776
- 777 Huneus, N., Schulz, M., Balkanski, Y., Griesfeller, J., Prospero, J., Kinne, S., Bauer, S.,  
778 Boucher, O., Chin, M., Dentener, F., Diehl, T., Easter, R., Fillmore, D., Ghan, S., Ginoux, P.,  
779 Grini, A., Horowitz, L., Koch, D., Krol, M. C., Landing, W., Liu, X., Mahowald, N., Miller, R.,  
780 Morcrette, J. J., Myhre, G., Penner, J., Perlwitz, J., Stier, P., Takemura, T., and Zender, C. S.  
781 (2011), Global dust model intercomparison in AeroCom phase I. *Atmospheric Chemistry and*  
782 *Physics*, 11, 7781-7816. 10.5194/acp-11-7781-2011  
783
- 784 Jaffe, D., Anderson, T., Covert, D., Kotchenruther, R., Trost, B., Danielson, J., Simpson, W.,  
785 Bernsten, T., Karlsdottir, S., Blake, D., Harris, J., Carmichael, G., and Uno, I. (1999), Transport  
786 of Asian air pollution to North America. *Geophysical Research Letters*, 26, 711-714.  
787 10.1029/1999GL900100  
788
- 789 Jickells, T., and Moore, C. M. (2015), The Importance of Atmospheric Deposition for Ocean  
790 Productivity. *Annual Review of Ecology, Evolution, and Systematics*, 46, 481-501.  
791 10.1146/annurev-ecolsys-112414-054118  
792
- 793 Kanakidou, M., Duce, R. A., Prospero, J. M., Baker, A. R., Benitez-Nelson, C., Dentener, F. J.,  
794 Hunter, K. A., Liss, P. S., Mahowald, N., Okin, G. S., Sarin, M., Tsigaridis, K., Uematsu, M.,  
795 Zamora, L. M., and Zhu, T. (2012), Atmospheric fluxes of organic N and P to the global ocean.  
796 *Global Biogeochemical Cycles*, 26, GB3026. 10.1029/2011gb004277  
797
- 798 Kettle, A. J., Andreae, M. O., Amouroux, D., Andreae, T. W., Bates, T. S., Berresheim, H.,  
799 Bingemer, H., Boniforti, R., Curran, M. A. J., DiTullio, G. R., Helas, G., Jones, G. B., Keller, M.

- 800 D., Kiene, R. P., Leck, C., Levasseur, M., Malin, G., Maspero, M., Matrai, P., McTaggart, A. R.,  
801 Mihalopoulos, N., Nguyen, B. C., N 258ovo, A., Putaud, J. P., Rapsomanikis, S., Roberts, G.,  
802 Schebeske, G., Sharma, S., Simó, R., Staubes, R., Turner, S., and Uher, G. (1999), A global  
803 database of sea surface dimethylsulfide (DMS) measurements and a procedure to predict sea  
804 surface DMS as a function of latitude, longitude, and month. *Global Biogeochemical Cycles*, 13,  
805 399-444. 10.1029/1999gb900004  
806
- 807 Kocak, M., Kubilay, N., Herut, B., and Nimmo, M. (2005), Dry atmospheric fluxes of trace  
808 metals (Al, Fe, Mn, Pb, Cd, Zn, Cu) over the Levantine Basin: A refined assessment.  
809 *Atmospheric Environment*, 39, 7330-7341. 10.1016/j.atmosenv.2005.09.010  
810
- 811 Koelliker, Y., Totten, L. A., Gigliotti, C. L., Offenber, J. H., Reinfelder, J. R., Zhuang, Y., and  
812 Eisenreich, S. J. (2004), Atmospheric Wet Deposition of Total Phosphorus in New Jersey.  
813 *Water, Air, & Soil Pollution*, 154, 139-150. 10.1023/B:WATE.0000022952.12577.c5  
814
- 815 Krishnamurthy, A., Moore, J. K., Mahowald, N., Luo, C., and Zender, C. S. (2010), Impacts of  
816 atmospheric nutrient inputs on marine biogeochemistry. *Journal of Geophysical Research*, 115,  
817 G01006. 10.1029/2009jg001115  
818
- 819 Krom, M. D., Kress, N., Brenner, S., and Gordon, L. I. (1991), Phosphorus limitation of primary  
820 productivity in the eastern Mediterranean Sea. *Limnology and Oceanography*, 36, 424-432.  
821 10.4319/lo.1991.36.3.0424  
822
- 823 Krom, M. D., Thingstad, T. F., Brenner, S., Carbo, P., Drakopoulos, P., Fileman, T. W., Flaten,  
824 G. A. F., Groom, S., Herut, B., Kitidis, V., Kress, N., Law, C. S., Liddicoat, M. I., Mantoura, R.  
825 F. C., Pasternak, A., Pitta, P., Polychronaki, T., Psarra, S., Rassoulzadegan, F., Skjoldal, E. F.,  
826 Spyres, G., Tanaka, T., Tselepidis, A., Wassmann, P., Wexels Riser, C., Woodward, E. M. S.,  
827 Zodiatis, G., and Zohary, T. (2005), Summary and overview of the CYCLOPS P addition  
828 Lagrangian experiment in the Eastern Mediterranean. *Deep Sea Research Part II: Topical  
829 Studies in Oceanography*, 52, 3090-3108. 10.1016/j.dsr2.2005.08.018  
830
- 831 Krom, M. D., Emeis, K. C., and Van Cappellen, P. (2010), Why is the Eastern Mediterranean  
832 phosphorus limited? *Progress in Oceanography*, 55, 236-244. 10.1016/j.pocean.2010.03.003  
833
- 834 Laghdass, M., Catala, P., Caparros, J., Oriol, L., Lebaron, P., and Obernosterer, I. (2012), High  
835 contribution of SAR11 to microbial activity in the north west Mediterranean Sea. *Microb Ecol*,  
836 63, 324-333. 10.1007/s00248-011-9915-7  
837
- 838 Lelieveld, J., Crutzen, P. J., Ramanathan, V., Andreae, M. O., Brenninkmeijer, C. A. M.,  
839 Campos, T., Cass, G. R., Dickerson, R. R., Fischer, H., de Gouw, J. A., Hansel, A., Jefferson, A.,  
840 Kley, D., de Laat, A. T. J., Lal, S., Lawrence, M. G., Lobert, J. M., Mayol-Bracero, O. L., Mitra,  
841 A. P., Novakov, T., Oltmans, S. J., Prather, K. A., Reiner, T., Rodhe, H., Scheeren, H. A., Sikka,  
842 D., and Williams, J. (2001), The Indian Ocean Experiment: Widespread Air Pollution from  
843 South and Southeast Asia. *Science*, 291, 1031-1036. 10.1126/science.1057103  
844

- 845 Lutz, S., Anesio, A. M., Raiswell, R., Edwards, A., Newton, R. J., Gill, F., and Benning, L. G.  
846 (2016), The biogeography of red snow microbiomes and their role in melting arctic glaciers.  
847 *Nature Comms*, 7, 11968. 10.1038/ncomms11968  
848
- 849 Mahowald, N., Jickells, T. D., Baker, A. R., Artaxo, P., Benitez-Nelson, C. R., Bergametti, G.,  
850 Bond, T. C., Chen, Y., Cohen, D. D., Herut, B., Kubilay, N., Losno, R., Luo, C., Maenhaut, W.,  
851 McGee, K. A., Okin, G. S., Siefert, R. L., and Tsukuda, S. (2008), Global distribution of  
852 atmospheric phosphorus sources, concentrations and deposition rates, and anthropogenic  
853 impacts. *Global Biogeochemical Cycles*, 22, GB4026. 10.1029/2008gb003240  
854
- 855 Mahowald, N. M. (2004), Comment on “Relative importance of climate and land use in  
856 determining present and future global soil dust emission” by I. Tegen et al. *Geophysical*  
857 *Research Letters*, 31, L24105. 10.1029/2004gl021272  
858
- 859 Maki, T., Ishikawa, A., Mastunaga, T., Pointing, S. B., Saito, Y., Kasai, T., Watanabe, K., Aoki,  
860 K., Horiuchi, A., Lee, K. C., Hasegawa, H., Iwasaka, Y. (2016), Atmospheric aerosol deposition  
861 influences marine microbial communities in oligotrophic surface waters of the western Pacific  
862 Ocean. *Deep-Sea Research*, 118, 37-45. 10.1016/j.dsr.2016.10.002  
863
- 864 Mann, G. W., Carslaw, K. S., Spracklen, D. V., Ridley, D. A., Manktelow, P. T., Chipperfield,  
865 M. P., Pickering, S. J., and Johnson, C. E. (2010), Description and evaluation of GLOMAP-  
866 mode: a modal global aerosol microphysics model for the UKCA composition-climate model.  
867 *Geoscientific Model Development*, 3, 519-551. 10.5194/gmd-3-519-2010  
868
- 869 Markaki, Z., Oikonomou, K., Kocak, M., Kouvarakis, G., Chaniotaki, A., Kubilay, N., and  
870 Mihalopoulos, N. (2003), Atmospheric deposition of inorganic phosphorus in the Levantine  
871 Basin, eastern Mediterranean: Spatial and temporal variability and its role in seawater  
872 productivity. *Limnology and Oceanography*, 48, 1557-1568. 10.4319/lo.2003.48.4.1557  
873
- 874 Markaki, Z., Loÿe-Pilot, M. D., Violaki, K., Benyahya, L., Mihalopoulos, N. (2010), Variability  
875 of atmospheric deposition of dissolved nitrogen and phosphorus in the Mediterranean and  
876 possible link to the anomalous seawater N/P ratio. *Marine Chemistry*, 120, 187-194.  
877 10.1016/j.marchem.2008.10.005  
878
- 879 Migon, C., & Sandroni, V. (1999), Phosphorus in rainwater: Partitioning inputs and impact on  
880 the surface coastal ocean. *Limnology and Oceanography*, 44, 1160-1165.  
881 10.4319/lo.1999.44.4.1160  
882
- 883 Mills, M. M., Ridame, C., Davey, M., La Roche, J., Geider, R. J. (2004), Iron and phosphorus  
884 co-limit nitrogen fixation in the eastern tropical North Atlantic. *Nature*, 429, 292-294.  
885 10.1038/nature02550  
886
- 887 Morales-Baquero, R., Pulido-Villena, E., and Reche, I. (2006), Atmospheric inputs of  
888 phosphorus and nitrogen to the southwest Mediterranean region: Biogeochemical responses of  
889 high mountain lakes. *Limnology and Oceanography*, 51, 830-837. 10.4319/lo.2006.51.2.0830  
890

- 891 Moutin, T., & Raimbault, P. (2002), Primary production, carbon export and nutrients availability  
892 in western and eastern Mediterranean Sea in early summer 1996 (MINOS cruise). *Journal of*  
893 *Marine Systems*, 33-34, 273-288. 10.1016/S0924-7963(02)00062-3  
894
- 895 Myriokefalitakis, S., Nenes, A., Baker, A. R. (2016), Mihalopoulos, N., and Kanakidou, M.:  
896 Bioavailable atmospheric phosphorous supply to the global ocean: a 3-D global modeling study.  
897 *Biogeosciences*, 13, 6519-6543. 10.5194/bg-13-6519-2016  
898
- 899 NADP/AIRMoN: (Atmospheric Integrated Research Monitoring Network), (2010), National  
900 Atmospheric Deposition Program (NADP) Office, Illinois State Water Survey, 2204 Griffith Dr.,  
901 Champaign, IL, U.S., Website: <http://nadp.sws.uiuc.edu/AIRMoN/>  
902
- 903 Nenes, A., Krom, M. D., Mihalopoulos, N., Van Cappellen, P., Shi, Z., Bougiatioti, A., Zarmas,  
904 P., and Herut, B. (2011), Atmospheric acidification of mineral aerosols: a source of bioavailable  
905 phosphorus for the oceans. *Atmospheric Chemistry and Physics*, 11, 6265-6272. 10.5194/acp-11-  
906 6265-2011  
907
- 908 Neuer, S., Torres-Padrón, M. E., Gelado-Caballero, M. D., Rueda, M. J., Hernández-Brito, J.,  
909 Davenport, R., and Wefer, G. (2004), Dust deposition pulses to the eastern subtropical North  
910 Atlantic gyre: Does ocean's biogeochemistry respond? *Global Biogeochemical Cycles*, 18,  
911 GB4020. 10.1029/2004gb002228  
912
- 913 Nickovic, S., Vukovic, A., Vujadinovic, M., Djurdjevic, V., and Pejanovic, G. (2012), Technical  
914 Note: High-resolution mineralogical database of dust-productive soils for atmospheric dust  
915 modeling. *Atmospheric Chemistry and Physics*, 12, 845-855. 10.5194/acp-12-845-2012  
916
- 917 Nightingale, P. D., Malin, G., Law, C. S., Watson, A. J., Liss, P. S., Liddicoat, M. I., Boutin, J.,  
918 and Upstill-Goddard, R. C. (2000), In situ evaluation of air-sea gas exchange parameterizations  
919 using novel conservative and volatile tracers. *Global Biogeochemical Cycles*, 14, 373-387.  
920 10.1029/1999gb900091  
921
- 922 Okin, G. S., Baker, A. R., Tegen, I., Mahowald, N. M., Dentener, F. J., Duce, R. A., Galloway, J.  
923 N., Hunter, K., Kanakidou, M., Kubilay, N., Prospero, J. M., Sarin, M., Surapipith, V., Uematsu,  
924 M., and Zhu, T. (2011), Impacts of atmospheric nutrient deposition on marine productivity:  
925 Roles of nitrogen, phosphorus, and iron. *Global Biogeochemical Cycles*, 25, GB2022.  
926 10.1029/2010gb003858  
927
- 928 Oredalen, T., Aas, W., and Maenhaut, W. (2010), Atmospheric dry and wet deposition of  
929 phosphorus in southern Norway. In: *Data obtained from the World Meteorological Organization*  
930 *Scientific Advisory Group of Precipitation Chemistry Workshop*, Berg-en-Dal, South Africa, 15-  
931 20 March 2010  
932
- 933 Ozsoy, T. (2003), Atmospheric wet deposition of soluble macro-nutrients in the Cilician Basin,  
934 north-eastern Mediterranean sea. *J Environ Monit*, 5, 971-976. 10.1039/B309636J  
935

- 936 Parkhurst, D. L., & Appelo, C. A. J. (2013), Description of input and examples for PHREEQC  
937 version 3 - A computer program for speciation, batch-reaction, one-dimensional transport, and  
938 inverse geochemical calculations. *U.S. Geological Survey Techniques and Methods*, Book 6  
939
- 940 Pey, J., Querol, X., Alastuey, A., Forastiere, F., and Stafoggia, M. (2013), African dust outbreaks  
941 over the Mediterranean Basin during 2001-2011: PM<sub>10</sub> concentrations, phenomenology and  
942 trends, and its relation with synoptic and mesoscale meteorology. *Atmospheric Chemistry and  
943 Physics*, 13, 1395-1410. 10.5194/acp-13-1395-2013  
944
- 945 Powley, H. R., Krom, M. D., and Van Cappellen, P. (2017), Understanding the unique  
946 biogeochemistry of the Mediterranean Sea: Insights from a coupled phosphorus and nitrogen  
947 model. *Global Biogeochemical Cycles*, 31, 1010-1031. 10.1002/2017gb005648  
948
- 949 Rengarajan, R., and Sarin, M. M. (2004), Atmospheric deposition fluxes of <sup>7</sup>Be, <sup>210</sup>Pb and  
950 chemical species to the Arabian Sea and Bay of Bengal. *Indian Journal of Marine Sciences*, 33,  
951 56-64.  
952
- 953 Ridame, C., Dekaezemacker, J., Guieu, C., Bonnet, S., L'Helguen, S., and Malien, F. (2014),  
954 Contrasted Saharan dust events in LNLC environments: impact on nutrient dynamics and  
955 primary production. *Biogeosciences*, 11, 4783-4800. 10.5194/bg-11-4783-2014  
956
- 957 Rodríguez, S., Alastuey, A., Alonso-Pérez, S., Querol, X., Cuevas, E., Abreu-Afonso, J., Viana,  
958 M., Pérez, N., Pandolfi, M., and de la Rosa, J. (2011), Transport of desert dust mixed with North  
959 African industrial pollutants in the subtropical Saharan Air Layer. *Atmospheric Chemistry and  
960 Physics*, 11, 6663-6685. 10.5194/acp-11-6663-2011  
961
- 962 Ruttenberg, K. C. (2003), The Global Phosphorus Cycle. *Treatise on Geochemistry*, 8, 585-643.  
963 10.1016/B0-08-043751-6/08153-6  
964
- 965 Sedwick, P. N., Sholkovitz, E. R., and Church, T. M. (2007), Impact of anthropogenic  
966 combustion emissions on the fractional solubility of aerosol iron: Evidence from the Sargasso  
967 Sea. *Geochemistry, Geophysics, Geosystems*, 8, Q10Q06. 10.1029/2007gc001586  
968
- 969 Shangguan, W., Dai, Y., Duan, Q., Liu, B., and Yuan, H. (2014), A global soil data set for earth  
970 system modeling. *Journal of Advances in Modeling Earth Systems*, 6, 249-263.  
971 10.1002/2013ms000293  
972
- 973 Sinha, P., Jaeglé, L., Hobbs, P. V., and Liang, Q. (2004), Transport of biomass burning  
974 emissions from southern Africa. *Journal of Geophysical Research: Atmospheres*, 109, D20204.  
975 10.1029/2004JD005044  
976
- 977 Slinn, W. G. N. (1982), Predictions for particle deposition to vegetative canopies. *Atmospheric  
978 Environment*, 16, 1785-1794. 10.1016/0004-6981(82)90271-2  
979



- 980 Smits, M. M., Bonneville, S., Benning, L. G., Banwart, S. A., Leake, J. R. (2012), Plant-driven  
981 weathering of apatite – the role of an ectomycorrhizal fungus. *Geobiology*, 10, 445-456.  
982 10.1111/j.1472-4669.2012.00331.x  
983
- 984 Srinivas, B., & Sarin, M. M. (2015), Atmospheric deposition of phosphorus to the Northern  
985 Indian Ocean. *Current Science*, 108, 1300-1305. 10.1016/j.scitotenv.2013.03.068  
986
- 987 Stibal, M., Anesio, A. M., Blues, C. J. D., Tranter, M. (2009), Phosphatase activity and organic  
988 phosphorus turnover on a high Arctic glacier. *Biogeosciences*, 6, 913-922. 10.5194/bg-6-913-  
989 2009  
990
- 991 Stockdale, A., Krom, M. D., Mortimer, R. J., Benning, L. G., Carslaw, K. S., Herbert, R. J., Shi,  
992 Z., Myriokefalitakis, S., Kanakidou, M., and Nenes, A. (2016), Understanding the nature of  
993 atmospheric acid processing of mineral dusts in supplying bioavailable phosphorus to the oceans.  
994 *Proc Natl Acad Sci USA*, 113, 14639-14644. 10.1073/pnas.1608136113  
995
- 996 Tamatamah, R. A., Hecky, R. E., and Duthie, H. (2005), The atmospheric deposition of  
997 phosphorus in Lake Victoria (East Africa). *Biogeochemistry*, 73, 325-344. 10.1007/s10533-004-  
998 0196-9  
999
- 1000 Thingstad, T. F., Krom, M. D., Mantoura, R. F., Flaten, G. A., Groom, S., Herut, B., Kress, N.,  
1001 Law, C. S., Pasternak, A., Pitta, P., Psarra, S., Rassoulzadegan, F., Tanaka, T., Tselepidis, A.,  
1002 Wassmann, P., Woodward, E. M., Riser, C. W., Zodiatis, G., and Zohary, T. (2005), Nature of  
1003 phosphorus limitation in the ultraoligotrophic eastern Mediterranean. *Science*, 309, 1068-1071.  
1004 10.1126/science.1112632  
1005
- 1006 Tipping, E., Benham, S., Boyle, J. F., Crow, P., Davies, J., Fischer, U., Guyatt, H., Helliwell, R.,  
1007 Jackson-Blake, L., Lawlor, A. J., Monteith, D. T., Rowe, E. C., and Toberman, H. (2014),  
1008 Atmospheric deposition of phosphorus to land and freshwater. *Environ Sci Process Impacts*, 16,  
1009 1608-1617. 10.1039/c3em00641g  
1010
- 1011 Tyrrell, T. (1999), The relative influences of nitrogen and phosphorus on oceanic primary  
1012 production. *Nature*, 400, 525-531. 10.1038/22941  
1013
- 1014 van der Werf, G. R., Randerson, J. T., Giglio, L., Collatz, G. J., Mu, M., Kasibhatla, P. S.,  
1015 Morton, D. C., DeFries, R. S., Jin, Y., and van Leeuwen, T. T. (2010), Global fire emissions and  
1016 the contribution of deforestation, savanna, forest, agricultural, and peat fires (1997–2009).  
1017 *Atmospheric Chemistry and Physics*, 10, 11707-11735. 10.5194/acp-10-11707-2010  
1018
- 1019 Vergara-Temprado, J., Murray, B. J., Wilson, T. W., amp, apos, Sullivan, D., Browse, J., Pringle,  
1020 K. J., Ardon-Dryer, K., Bertram, A. K., Burrows, S. M., Ceburnis, D., DeMott, P. J., Mason, R.  
1021 H., amp, apos, Dowd, C. D., Rinaldi, M., and Carslaw, K. S. (2017), Contribution of feldspar and  
1022 marine organic aerosols to global ice nucleating particle concentrations. *Atmospheric Chemistry  
1023 and Physics*, 17, 3637-3658. 10.5194/acp-17-3637-2017  
1024

- 1025 Vet, R., Artz, R. S., Carou, S., Shaw, M., Ro, C.-U., Aas, W., Baker, A., Bowersox, V. C.,  
1026 Dentener, F., Galy-Lacaux, C., Hou, A., Pienaar, J. J., Gillett, R., Forti, M. C., Gromov, S., Hara,  
1027 H., Khodzher, T., Mahowald, N. M., Nickovic, S., Rao, P. S. P., and Reid, N. W. (2014), A  
1028 global assessment of precipitation chemistry and deposition of sulfur, nitrogen, sea salt, base  
1029 cations, organic acids, acidity and pH, and phosphorus. *Atmospheric Environment*, 93, 3-100.  
1030 10.1016/j.atmosenv.2013.10.060  
1031  
1032 Wang, R., Balkanski, Y., Bopp, L., Aumont, O., Boucher, O., Ciais, P., Gehlen, M., Penuelas, J.,  
1033 Ethe, C., Hauglustaine, D., Li, B., Liu, J., Zhou, F., and Tao, S. (2015), Influence of  
1034 anthropogenic aerosol deposition on the relationship between oceanic productivity and warming.  
1035 *Geophys Res Lett*, 42, 10745-10754. 10.1002/2015GL066753  
1036  
1037 Wu, J., Sunda, W., Boyle, E. A., and Karl, D. M. (2000), Phosphate depletion in the western  
1038 North Atlantic Ocean. *Science*, 289, 759-762. 10.1126/science.289.5480.759  
1039  
1040 Yang, X., Post, W. M., Thornton, P. E., and Jain, A. (2013), The distribution of soil phosphorus  
1041 for global biogeochemical modeling. *Biogeosciences*, 10, 2525-2537. 10.5194/bg-10-2525-2013  
1042  
1043 Yogevev, T., Rahav, E., Bar-Zeev, E., Man-Aharonovich, D., Stambler, N., Kress, N., Béjà, O.,  
1044 Mulholland, M. R., Herut, B., Berman-Frank, I. (2011), Is dinitrogen fixation significant in the  
1045 Levantine Basin, East Mediterranean Sea? *Environmental Microbiology*, 13, 854-871.  
1046 doi:10.1111/j.1462-2920.2010.02402.x  
1047  
1048 Zamora, L. M., Prospero, J. M., Hansell, D. A., and Trapp, J. M. (2013), Atmospheric P  
1049 deposition to the subtropical North Atlantic: sources, properties, and relationship to N  
1050 deposition. *Journal of Geophysical Research: Atmospheres*, 118, 1546-1562. 10.1002/jgrd.50187  
1051  
1052 Zhang, G., Zhang, J., and Liu, S. (2007), Characterization of nutrients in the atmospheric wet and  
1053 dry deposition observed at the two monitoring sites over Yellow Sea and East China Sea.  
1054 *Journal of Atmospheric Chemistry*, 57, 41-57. 10.1007/s10874-007-9060-3  
1055  
1056 Zhang, Y., Mahowald, N., Scanza, R. A., Journet, E., Desboeufs, K., Albani, S., Kok, J. F.,  
1057 Zhuang, G., Chen, Y., Cohen, D. D., Paytan, A., Patey, M. D., Achterberg, E. P., Engelbrecht, J.  
1058 P., and Fomba, K. W. (2015), Modeling the global emission, transport and deposition of trace  
1059 elements associated with mineral dust. *Biogeosciences*, 12, 5771-5792. 10.5194/bg-12-5771-  
1060 2015  
1061  
1062

1063 **Tables**

1064

1065 Table 1. Absolute mass of bioavailable phosphorus (total and from each source) and dust  
 1066 components deposited to the surface of each region in the simulated year. All units are in  
 1067 Gg-P yr<sup>-1</sup> except for dust which is in Tg yr<sup>-1</sup>. Values in parentheses give annual mass per unit  
 1068 area in µg-P m<sup>-2</sup>yr<sup>-1</sup> except for dust which is in mg m<sup>-2</sup>yr<sup>-1</sup>.

Region	Bioavailable phosphorus deposition			Deposited dust content	
	Total (Bio-P)	from acid dissolution (Acid-P)	from labile pool (Lab-P)	Total phosphorus (TP)	Total dust *
<b>Ice sheets</b>					
Greenland	0.03 (18)	0.03 (15)	0.01 (3)	0.06 (30)	0.11 (57)
Antarctic	0.05 (3)	0.04 (3)	0.01 (1)	0.09 (6)	0.12 (8)
<b>Oceans and Seas</b>					
Arctic Ocean	0.5 (36)	0.4 (29)	0.1 (7)	0.9 (66)	1.7 (123)
Pacific					
NE	2.5 (66)	1.8 (51)	0.5 (15)	5.2 (147)	10.7 (303)
Ocean					
SE	0.8 (14)	0.6 (11)	0.1 (3)	1.5 (26)	3.0 (53)
NW	3.6 (87)	2.7 (65)	0.9 (22)	9.5 (230)	22.1 (535)
SW	1.2 (38)	0.9 (30)	0.2 (8)	2.6 (86)	5.9 (192)
Atlantic					
NE	6.9 (436)	2.0 (125)	4.9 (310)	48.4 (3041)	103.4 (6497)
Ocean					
SE	2.1 (70)	1.6 (52)	0.5 (18)	5.5 (184)	10.9 (360)
NW	4.7 (181)	2.2 (84)	2.5 (98)	24.5 (943)	50.8 (1959)
SW	1.1 (95)	0.6 (56)	0.4 (39)	4.9 (431)	7.8 (689)
Baltic Sea	0.05 (146)	0.03 (105)	0.01 (40)	0.13 (391)	0.23 (689)
Mediterranean Sea	1.5 (549)	0.5 (177)	1.0 (372)	9.8 (3592)	16.3 (5962)
Indian					
W	3.5 (89)	1.5 (39)	2.0 (50)	20.2 (516)	42.0 (1074)
Ocean					
E	2.2 (62)	1.4 (39)	0.8 (23)	8.7 (245)	19.7 (559)
South China Sea	0.5 (68)	0.4 (54)	0.1 (14)	1.2 (148)	2.7 (327)
Southern Ocean	0.3 (14)	0.2 (11)	0.1 (3)	0.6 (31)	1.0 (53)
<b>Continents</b>					
Europe	3.5 (364)	1.9 (199)	1.6 (165)	15.4 (1612)	26.9 (2822)
North America	2.0 (87)	1.4 (62)	0.6 (25)	6.1 (270)	10.9 (483)
South America	3.3 (180)	1.4 (79)	1.8 (101)	19.4 (1074)	32.3 (1793)
Africa	51.6 (1738)	3.5 (119)	48.1 (1619)	466.8 (15725)	940.4 (31681)
Asia	23.6 (562)	4.6 (109)	19.0 (453)	198.5 (4725)	425.8 (10138)
Australia	2.3 (282)	0.5 (65)	1.7 (218)	19.9 (2480)	44.5 (5555)
Antarctica	0.05 (3)	0.04 (3)	0.01 (1)	0.09 (6)	0.12 (8)
<b>Totals</b>					
Global total	117 (229)	30 (59)	87 (170)	870 (1695)	1779 (3468)
Ocean total	31.2 (84)	16.9 (45)	14.3 (39)	144 (392)	298 (814)
Land total	86 (595)	13 (92)	73 (503)	726 (5013)	1481 (10225)

all units in Gg-P yr<sup>-1</sup> (µg-P m<sup>-2</sup>yr<sup>-1</sup>)  
 \* dust in Tg yr<sup>-1</sup> (mg m<sup>-2</sup>yr<sup>-1</sup>)

1069

1070

1071

1072

Table 2. Annual means: percentage of total-P in deposited dust bioavailable at surface; percentage of bioavailable-P from acid dissolution of apatite; percentage of total-P in dust from labile-P; and percentage of apatite-P in deposited dust dissolved by acid dissolution.

Region	% of TP in dust bioavailable at surface	% of bio-P from acid dissolution	% of TP in dust from labile pool	% of Ap-P in dust dissolved
<b>Ice sheets</b>				
Greenland	62 %	82 %	11 %	100 %
Antarctic	60 %	82 %	11 %	93 %
<b>Oceans and Seas</b>				

Arctic Ocean		55 %	81 %	10 %	86 %
Pacific Ocean	NE	45 %	77 %	10 %	73 %
	SE	52 %	81 %	10 %	84 %
	NW	38 %	75 %	10 %	56 %
	SW	44 %	80 %	9 %	65 %
Atlantic Ocean	NE	14 %	29 %	10 %	9 %
	SE	38 %	75 %	10 %	58 %
	NW	19 %	46 %	10 %	19 %
	SW	22 %	59 %	9 %	28 %
Baltic Sea		37 %	72 %	10 %	54 %
Mediterranean Sea		15 %	32 %	10 %	10 %
Indian Ocean	W	17 %	43 %	10 %	14 %
	E	25 %	63 %	9 %	31 %
South China Sea		46 %	79 %	10 %	70 %
Southern Ocean		45 %	79 %	10 %	74 %
<b>Continents</b>					
Europe		23 %	55 %	10 %	25 %
North America		32 %	71 %	9 %	45 %
South America		17 %	44 %	9 %	16 %
Africa		11 %	7 %	10 %	12 %
Asia		12 %	19 %	10 %	4 %
Australia		11 %	23 %	9 %	5 %
Antarctica		60 %	82 %	11 %	93 %
<b>Global means</b>					
Global mean		14 %	26 %	10 %	7 %
Ocean mean		22 %	54 %	10 %	24 %
Land mean		12 %	16 %	10 %	4 %

1073

1074 Table 3. Sensitivity of annual deposited mass of bioavailable phosphorus to degree of external  
 1075 mixing of apatite and calcium carbonate (CaCO<sub>3</sub>) content in the deposited dust. Data show  
 1076 percentage increase of bioavailable phosphorus compared to the control run (0% mixing;  
 1077 internally mixed assumption). An externally mixed percentage of 0% implies that apatite and  
 1078 dust are present at the same ratio in all dust particles (therefore internally mixed) and a  
 1079 percentage of 100% implies that apatite and calcium carbonate are exclusively present in  
 1080 different dust particles.

Region	Percentage of apatite and CaCO <sub>3</sub> externally mixed in dust						
	1%	2%	5%	10%	25%	50%	100%
<b>Ice sheets</b>							
Greenland	0	0	0	0	0	0	0
Antarctic	0	0	0	1	2	4	5
<b>Oceans and Seas</b>							
Arctic	0	0	1	2	4	7	11
Pacific	0	1	2	4	9	17	24
	SE	0	0	1	2	4	8
	NW	1	1	4	7	17	33
	SW	1	1	3	5	12	24
Atlantic	NE	3	6	15	31	77	153
	SE	1	1	3	6	15	29
	NW	2	4	10	20	51	102
	SW	2	3	8	16	39	78
Baltic		1	1	3	7	17	33

Mediterranean	3	6	15	29	73	148	221
Indian W	3	5	13	26	66	132	198
E	1	3	7	15	37	74	110
South China	0	1	2	4	9	19	27
Southern	0	1	2	3	8	16	23
<b>Ocean total</b>	<b>2</b>	<b>4</b>	<b>9</b>	<b>18</b>	<b>44</b>	<b>88</b>	<b>131</b>

all data in % increase compared to control run

1081  
 1082 Table 4. Modelled deposition fluxes of TP and Bio-P to different ocean basins in Gg-P yr<sup>-1</sup>.  
 1083 Figures in parentheses correspond to the TP bioavailability (%) upon deposition. Bio-P data from  
 1084 Zhang et al. (2015) are presented for their 'sol-1' dataset (please refer to the study for details).  
 1085 Values for both total dissolved phosphorus (DP) and dissolved inorganic phosphorus (DIP) from  
 1086 Myriokefalitakis et al. (2016) are included. Values from Zhang et al. (2015) and this study are  
 1087 only for phosphorus from inorganic mineral dust.

	Mahowald et al. 2008		Okin et al. 2011		Zhang et al. 2015*		Myriokefalitakis et al. 2016			This study*	
	TP	Bio-P	TP	Bio-P	TP	Bio-P sol-1	TP	Bio-P DP	Bio-P DIP †	TP	Bio-P
Atlantic	<b>232</b>	35.8 (15)	<b>128</b>	-	<b>112</b>	9.6 (9)	<b>110</b>	54.9 (50)	36.6	<b>83</b>	14.8 (18)
N Atlantic	<b>190</b>	27.9 (15)	-	-	<b>103</b>	8.8 (9)	<b>96</b>	44.2 (46)	32.3	<b>73</b>	11.6 (16)
S Atlantic	<b>42</b>	7.9 (19)	-	-	<b>9</b>	0.8 (9)	<b>14</b>	10.6 (74)	4.4	<b>10</b>	3.2 (30)
Pacific	<b>85</b>	28 (33)	<b>68</b>	-	<b>18</b>	1.8 (9)	<b>60</b>	48.4 (81)	26.6	<b>20</b>	8.4 (42)
N Pacific	<b>63</b>	22 (35)	-	-	<b>18</b>	1.7 (10)	<b>47</b>	38.0 (80)	23.9	<b>15</b>	5.9 (40)
S Pacific	<b>22</b>	6 (27)	-	-	<b>1</b>	0.07 (8)	<b>12</b>	10.5 (86)	2.7	<b>5</b>	2.5 (47)
Indian	<b>149</b>	20.3 (14)	<b>73</b>	-	<b>37</b>	3.8 (10)	<b>56</b>	37.3 (66)	20.7	<b>29</b>	5.7 (20)
Southern	<b>12</b>	1.7 (14)	<b>32</b>	-	<b>0.2</b>	0.01 (7)	<b>2</b>	1.5 (82)	0.2	<b>1</b>	0.5 (46)
Arctic	<b>7</b>	2.2 (32)	-	-	<b>1</b>	0.1 (10)	<b>5</b>	3.3 (74)	1.7	<b>1</b>	0.5 (55)
Mediterranean	<b>54</b>	5.7 (11)	-	-	<b>11</b>	1.1 (10)	<b>7</b>	4.4 (59)	2.7	<b>10</b>	1.5 (15)
Antarctic ice	-	-	-	-	<b>0.1</b>	0.01 (9)	<b>0.1</b>	0.0 (23)	0.0	<b>0.1</b>	0.1 (60)
Greenland ice	-	-	-	-	<b>5</b>	0.5 (9)	<b>0.3</b>	0.2 (62)	0.1	<b>0.1</b>	0.03 (62)
Ocean total	<b>558</b>	96.5 (17)	<b>320</b>	-	<b>180</b>	16.3 (9)	<b>240</b>	150.2 (63)	88.7	<b>144</b>	31.2 (22)
Land total	<b>831</b>	143.5 (17)	-	-	-	-	<b>1051</b>	303 (29)	160	<b>726</b>	86 (12)

\* mineral dust only

† dissolved inorganic P from dust and volcanic emissions only

1088  
 1089

1090 **Figure captions**

1091

1092 Figure 1. Global gridded datasets used for GLOMAP dust-associated emissions of **a)** total-  
1093 phosphorus (ppm); **b)** apatite-phosphorus (ppm); **c)** labile-phosphorus (ppm); **d)** calcium-  
1094 carbonate (%); **e)** ratio of apatite-phosphorus to total-phosphorus (%); and **f)** ratio of labile-  
1095 phosphorus to total-phosphorus (%).

1096

1097 Figure 2. Annual deposition rate of **a)** bioavailable phosphorus in  $\mu\text{g-P m}^{-2}\text{yr}^{-1}$ , **b)** dust in  
1098  $\text{g m}^{-2}\text{yr}^{-1}$ , and **c)** dust-associated  $\text{H}^+$  ions in  $\text{mol-H}^+ \text{m}^{-2}\text{yr}^{-1}$ .

1099

1100 Figure 3. Annual mean percentage contribution of **a)** the acid dissolution process and **b)** the  
1101 labile pool of phosphorus to the total bioavailable phosphorus from dust deposition, and **c)** the  
1102 percentage of the total phosphorus content in dust that is bioavailable upon deposition.

1103

1104 Figure 4. Modelled deposition fluxes (contours) and observations (filled circles) from Vet et al.  
1105 (2014) in  $\mu\text{g-P m}^{-2}\text{yr}^{-1}$  for **a)** wet-deposited TP, **b)** dry-deposited TP, **c)** wet-deposited Bio-P, and  
1106 **d)** dry-deposited Bio-P. Modelled and observational values follow the same color scale.

1107

1108 Figure 5. Data as in Figure 4 but shown as scatter plots with observations from Vet et al. (2014)  
1109 on the x-axis and modelled fluxes from this study on the y-axis. **a)** shows data for TP fluxes and  
1110 **b)** for Bio-P fluxes. Different colored circles depict different regions. Vertical lines in a) show  
1111 the standard deviation of modelled deposition flux at that location from the simulated year (not  
1112 repeated in b) for clarity). Crosses in b) show the modelled deposition flux of Bio-P without  
1113 simulated acid dissolution of apatite.

Figure 1.

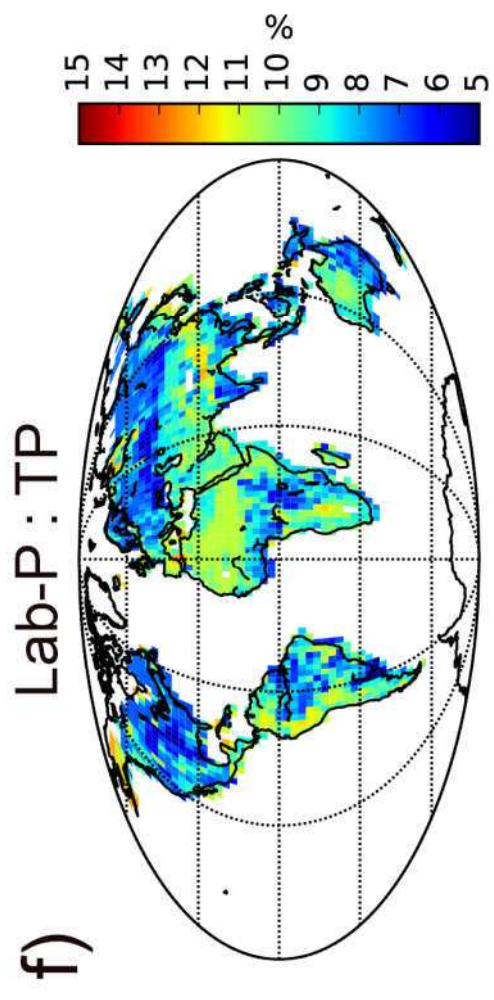
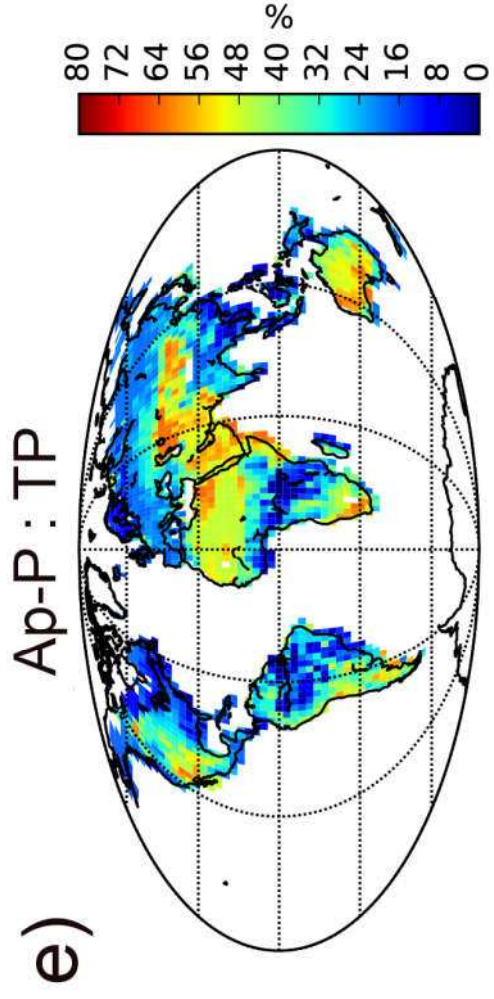
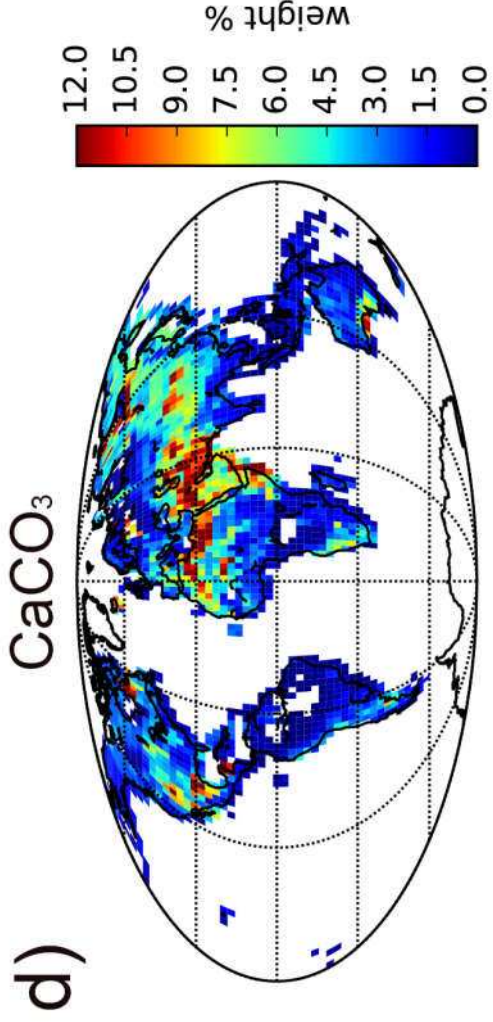
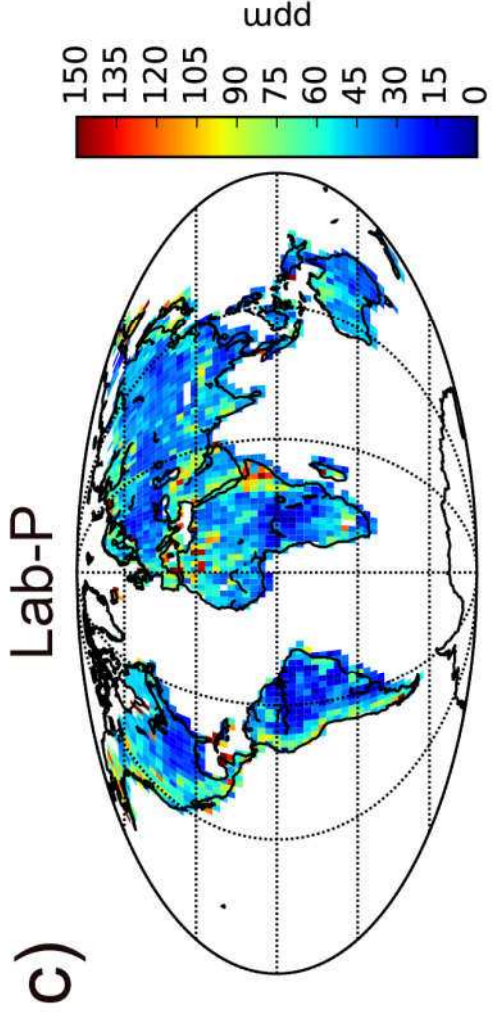
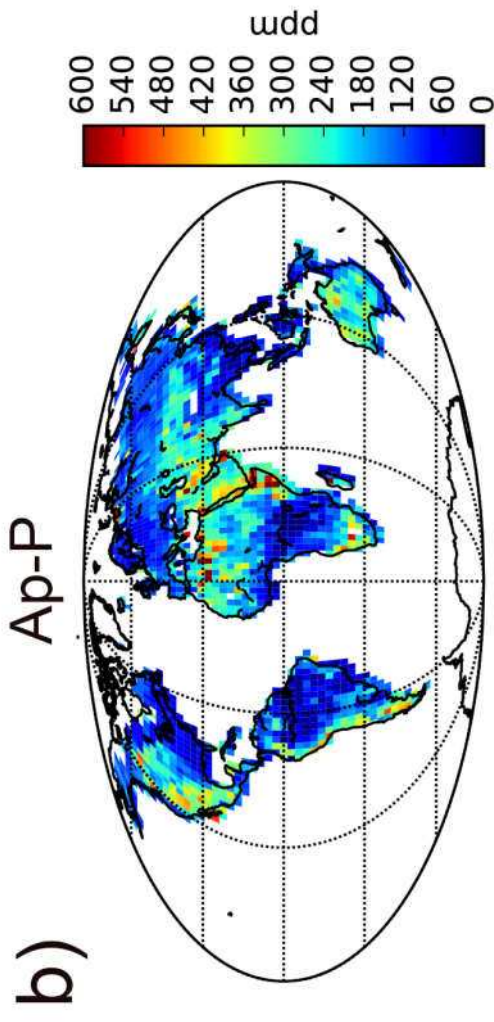
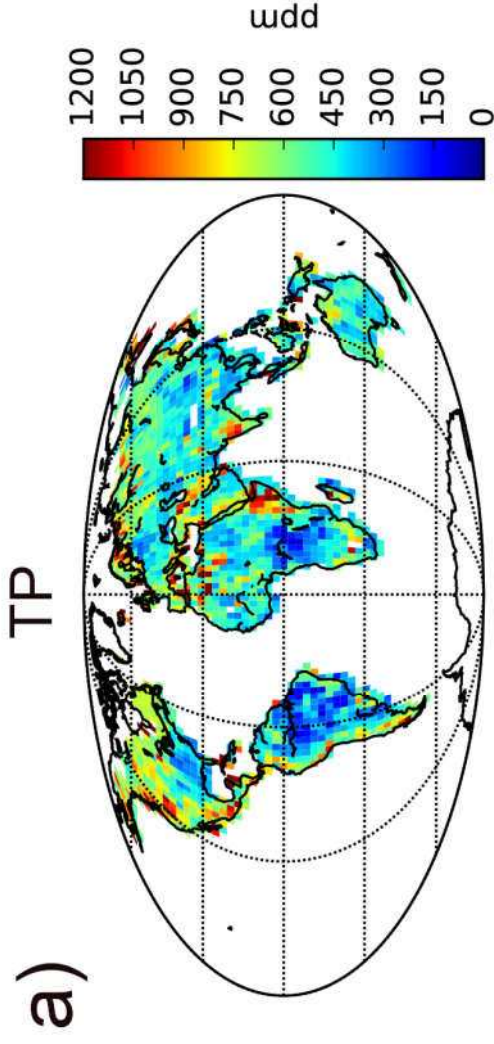




Figure 2.

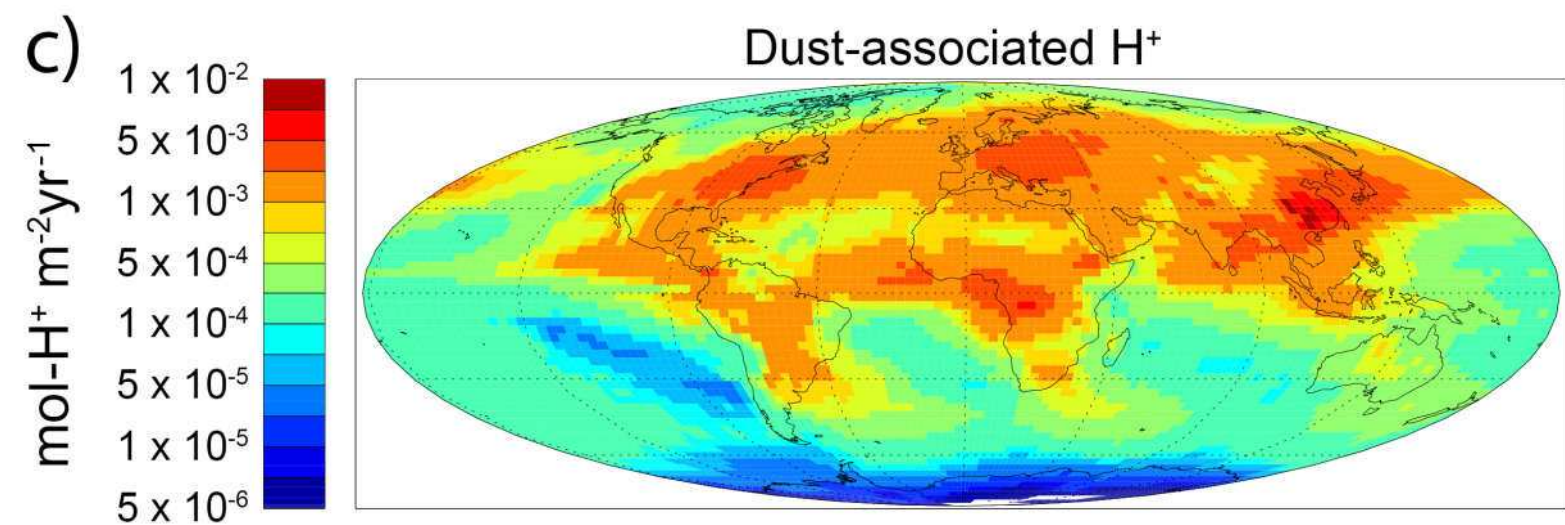
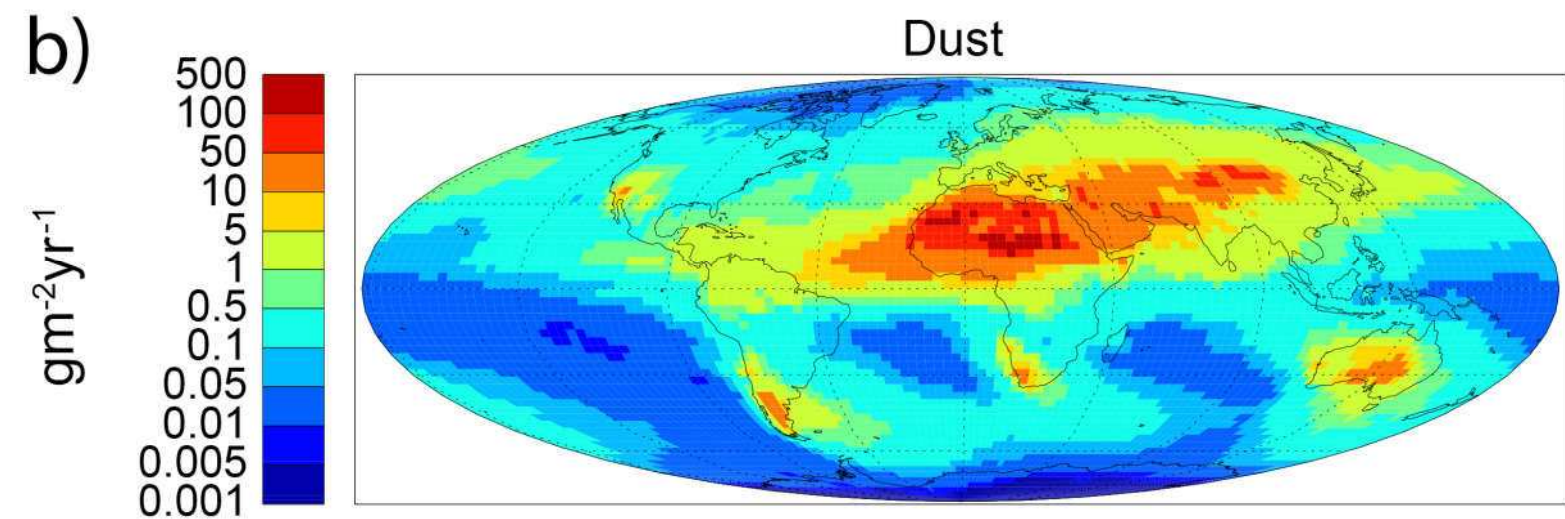
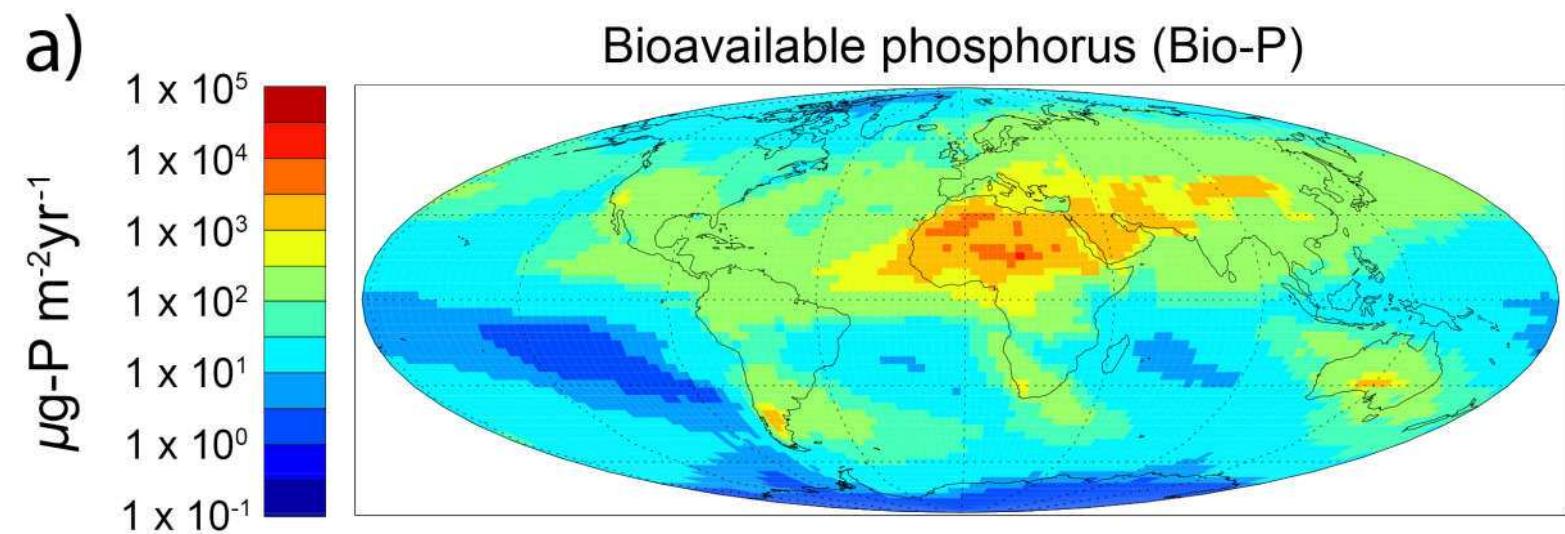
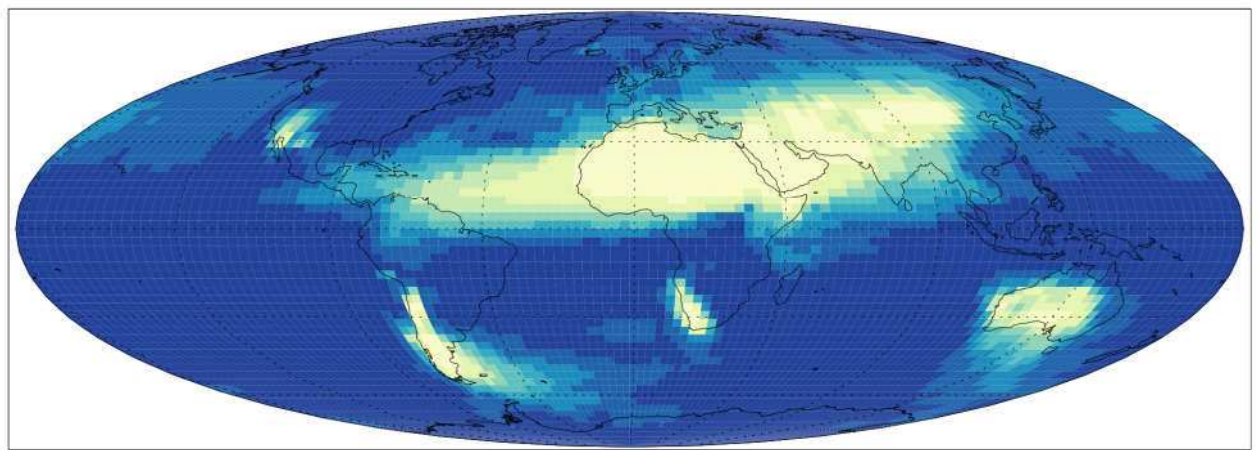
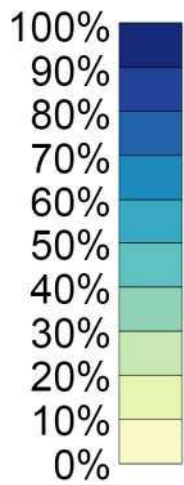


Figure 3.

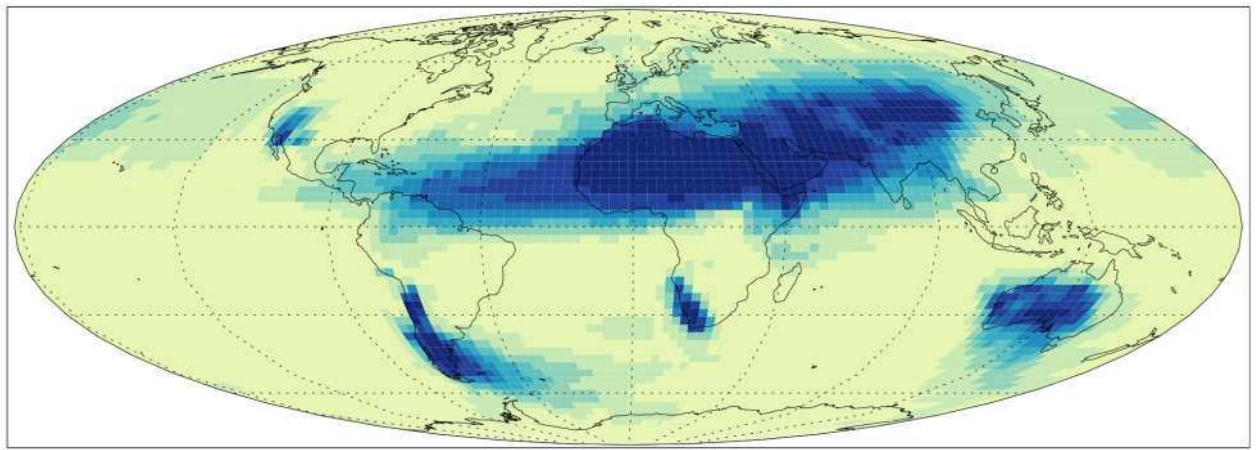
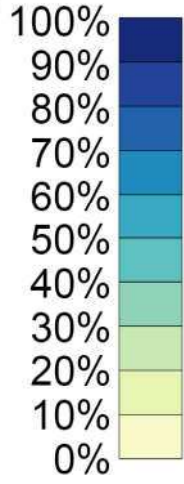
a)

Contribution of Acid-P to Bio-P



b)

Contribution of Lab-P to Bio-P



c)

Percentage of TP bioavailable at surface

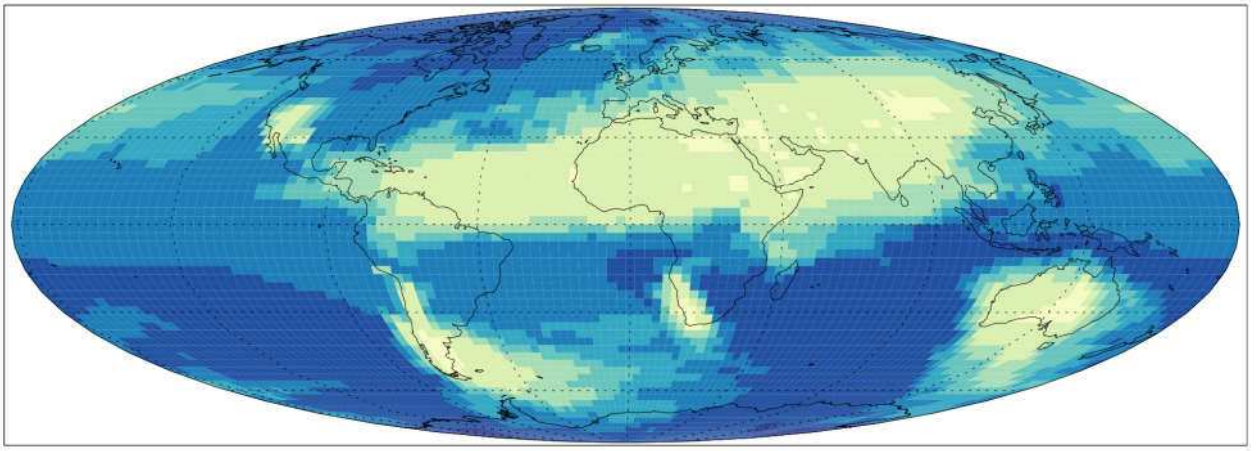
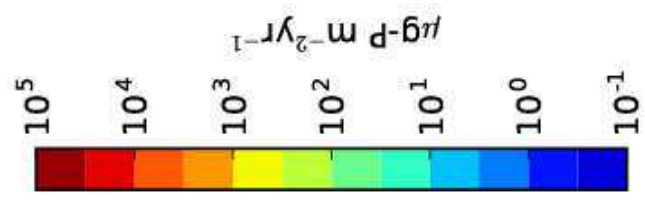
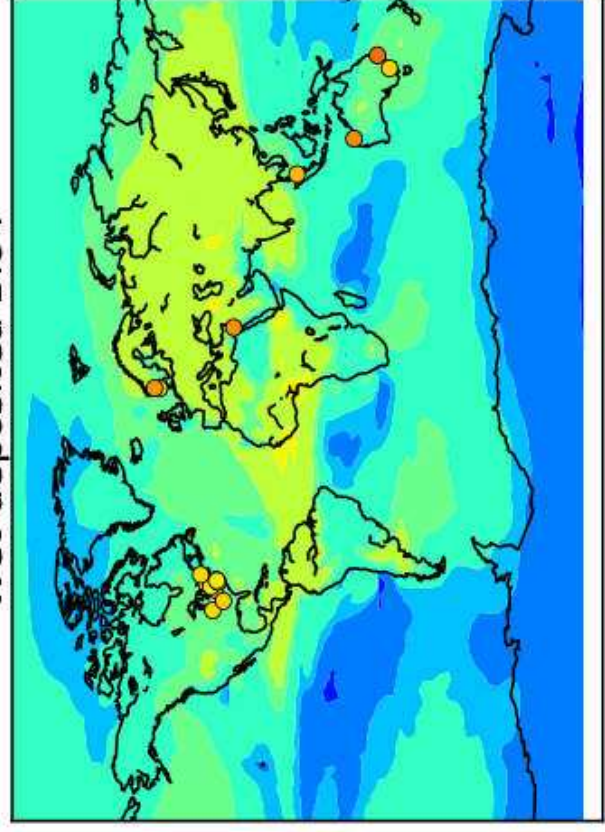


Figure 4.

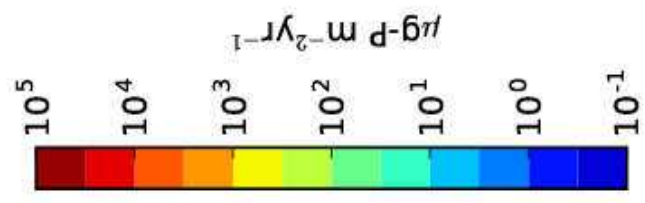
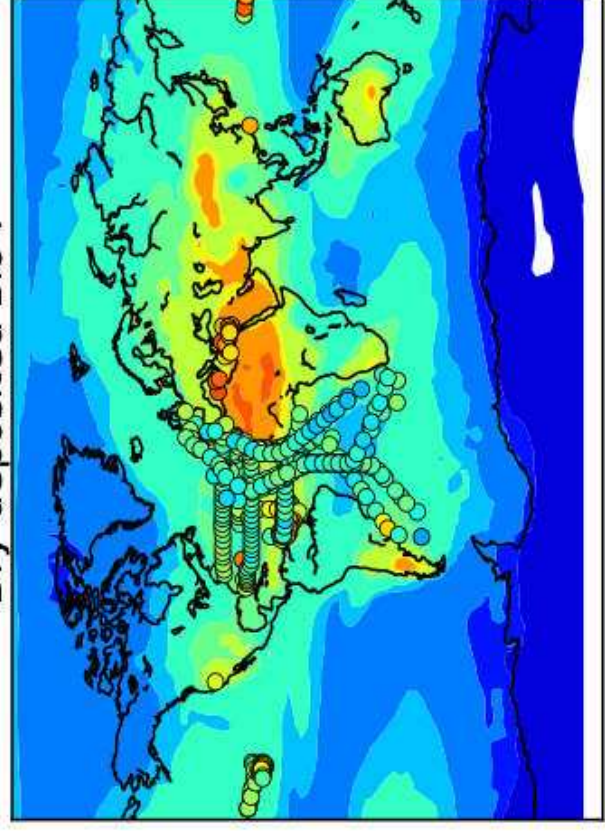
a)

Wet-deposited Bio-P



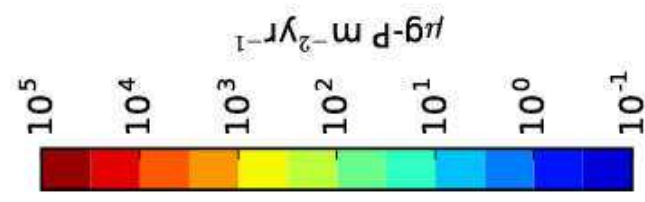
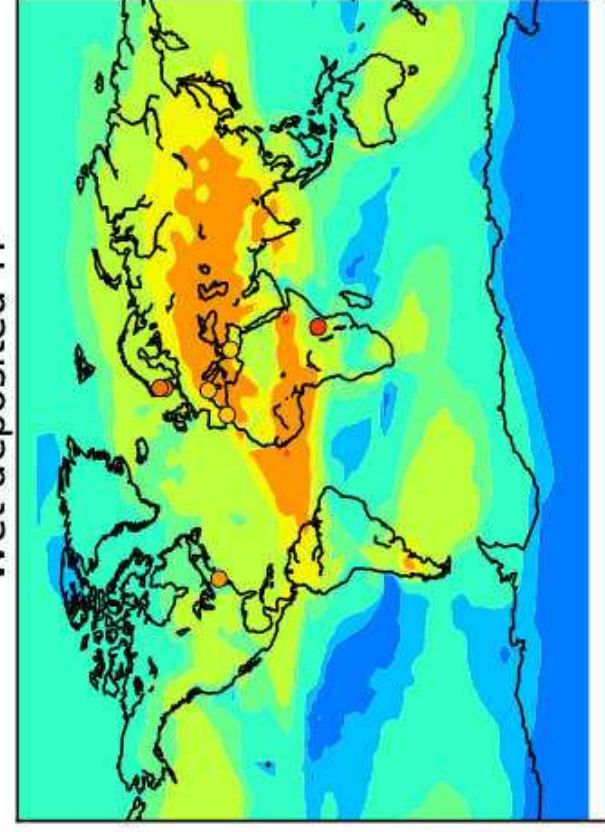
b)

Dry-deposited Bio-P



c)

Wet-deposited TP



d)

Dry-deposited TP

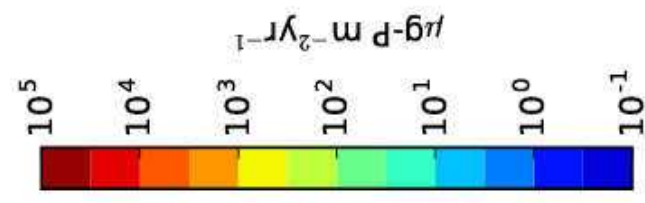
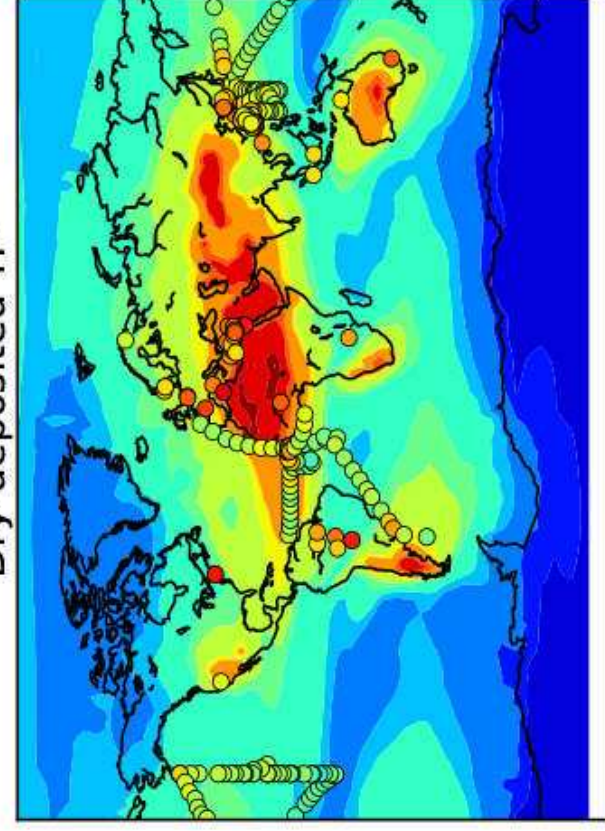


Figure 5.

